Oncogenic Ras Disrupts Epithelial Integrity by Activating the Transmembrane Serine Protease Hepsin

Tervonen, Topi A.

2021-03-15

Tervonen , T A , Pant , S M , Belitskin , D , Englund , J I , Närhi , K , Haglund , C , Kovanen , P E , Verschuren , E W & Klefström , J 2021 , ' Oncogenic Ras Disrupts Epithelial Integrity by Activating the Transmembrane Serine Protease Hepsin ' , Cancer Research , vol. 81 , no. 6 , pp. 1513-1527 . https://doi.org/10.1158/0008-5472.CAN-20-1760

http://hdl.handle.net/10138/341621
https://doi.org/10.1158/0008-5472.CAN-20-1760

acceptedVersion

Oncogenic Ras disrupts epithelial integrity by activating the transmembrane serine protease hepsin

Topi A. Tervonen[1], Shishir M. Pant[1], Denis Belitškin[1], Johanna I. Englund[1], Katja Närhi[1,2], Caj Haglund[3], Panu E. Kovanen[1,4], Emmy W. Verschuren[1,2], Juha Klefström[1]

1. Research Programs Unit/ Translational Cancer Medicine and Medicum, Faculty of Medicine, University of Helsinki, Biomedicum Helsinki 1, Rm B507, P.O. Box 63 (street address: Haartmaninkatu 8), 00014 University of Helsinki, Finland
2. Institute for Molecular Medicine Finland (FIMM), HiLIFE, P.O. Box 20, FI-00014 University of Helsinki, Finland
3. Research Programs Unit/ Translational Cancer Medicine Research Program and Department of Surgery, Clinicum, Faculty of Medicine, University of Helsinki, Biomedicum Helsinki 1, Rm B507, P.O. Box 63 (street address: Haartmaninkatu 8), 00014 University of Helsinki, Finland
4. Department of Pathology, HUSLAB and Haartman Institute, Helsinki University Central Hospital and University of Helsinki, Haartmaninkatu 3, P.O. Box 21, 00014 University of Helsinki, Finland

Running title: Oncogenic Ras breaks epithelial integrity via hepsin

Keywords: Breast cancer, protease activity, MAPK pathway, cell-cell junctions, cell-basement membrane junctions

Financial support: Academy of Finland, Finnish Cancer Organizations and TEKES. T.A.T. was funded by the Helsinki Institute of Life Science infrastructures of University of Helsinki.

Corresponding author:

Juha Klefström, PhD.,
Research Director, Translational Cancer Medicine Research Program, Faculty of Medicine, 00014 University of Helsinki, Finland.
Email juha.klefstrom@helsinki.fi
Tel +358-44-3773876, +358-2941-25493

Conflict of interest statement: The authors declare no competing interests.

ABSTRACT

Ras proteins play a causal role in human cancer by activating multiple pathways that promote cancer growth and invasion. However, little is known about how Ras induces the first diagnostic features of invasion in solid tumors, including loss of epithelial integrity and breaching of the basement membrane. In this study, we found that oncogenic Ras strongly promotes the activation of hepsin, a member of the hepsin/TMPRSS type II transmembrane serine protease family. Mechanistically, the Ras-dependent hepsin activation was mediated via Raf-MEK-ERK signaling, which controlled hepsin protein stability through the heat shock transcription factor-1 stress pathway. In Ras-transformed three-dimensional mammary epithelial culture, ablation of hepsin restored desmosomal cell-cell junctions, hemidesmosomes, and basement membrane integrity and epithelial cohesion. In tumor xenografts harboring mutant KRas, silencing of hepsin increased local invasion concomitantly with accumulation of collagen IV. These findings suggest that hepsin is a critical protease for Ras-dependent tumorigenesis, executing cell-cell and cell-matrix pathologies important for early tumor dissemination.

Statement of Significance

Findings identify the cell surface serine protease hepsin as a potential therapeutic target for its role in oncogenic Ras-mediated deregulation of epithelial cell-cell and cell-matrix interactions and cohesion of epithelial structure.

INTRODUCTION

During malignant tumor progression, the onset and maintenance of invasive phenotype not only requires cytoskeletal alterations to help cell motility, but also disassembly of the cell-cell and cell-matrix junctions to facilitate detachment of the cells or cell clusters from the tumor bulk. These cell-cell and cell-matrix pathologies also include dissolution of the basement membrane, which normally separates epithelial tissues from the stroma (1). While loss of the epithelial tissue structure and dissolution of the basement membrane (BM) are diagnostic hallmarks of all advanced epithelial cancers, the dynamics and mechanisms causing these histopathological changes are still poorly understood. At the cellular level, the intricate cell-cell and cell-matrix remodeling processes during invasion appear to involve concomitant or consequential cycles of loss and re-establishment of cell-cell and cell-matrix interactions to support better motility, survival and proliferation (2,3). It is generally held that these abrupt pro-tumorigenic alterations emerge from oncogene-driven erratic intracellular cytokine and growth factor signaling mechanisms, which act in conjunction with dysregulated pericellular protease systems (4).

Oncogenic activating mutations in Ras proteins are found in about one-third of human cancers; these mutations lock Ras into its active GTP-bound state, amplifying signaling through the Raf-MEK-ERK cascade (a.k.a. MAPK pathway) (5,6) (cBioportal). In addition to point mutations, also Ras gene amplifications, mutation-independent gain-of-function and other mechanisms commonly feed the downstream pathway in an abnormally persistent manner in epithelial cancers (6-12). The oncogenicity of Ras proteins was historically recognized in the context of cell transformation, typified by Ras-induced morphological changes in cultured fibroblasts due to altered cytoskeletal dynamics and cell adhesions (13,14). In two-dimensional (2D) monolayer cultures of epithelial cells, persistent Ras-MAPK signaling diminishes cell adhesion also by damaging epithelial-specific cell-cell junctions. For example, Ras destabilizes adherence junctions by downregulating E-cadherin and ß-catenin (15). In addition, Ras-induced loss of occludin, claudin-1 and ZO-1 interferes with tight junction formation (16) and Ras-dependent dissociation of desmoplakin from the cell periphery disrupts desmosomes (17).

In three-dimensional (3D) organotypic epithelial cultures, a hyperactive Ras pathway leads to loss of apicobasal cell polarity and disruption of epithelial architecture, which events associate not only with deficiencies in adherence junctions and tight junctions but also with loss of the α6-integrin and laminin components of the BM. The Ras-transformed disorganized epithelial 3D structures have been shown to feature groups of motile cells that form multicellular protrusions, resembling invasive processes (18-21).

While oncogenic activation of the Ras pathway alone is sufficient to break epithelial cohesion and induce dissolution of BM, little is known how Ras establishes these cell-cell and cell-matrix pathologies during epithelial tumor progression. Oncogenic Ras is known to activate a number of proteases, including matrix metalloproteinases (MMPs), plasminogen activators, and cathepsins (22,23). In particular, downstream of Ras, the MAPK pathway has been coupled to activation of MMP-9 and consequent cleavage of the BM protein laminin-111 (21). However, besides possible involvement of MMPs, little is known of the mechanisms that couple active Ras to the pericellular cancer degradome.

Here, we find that oncogenic Ras proteins induce via the MAPK mediated HSF1 stress pathway a strong activation of the type II transmembrane serine protease hepsin, which is an epithelial protease widely overexpressed in prostate, breast, ovarian, renal cell, and endometrial cancer (24-29). Strikingly, ablation of hepsin in Ras-transformed 3D epithelial structures leads to restoration of epithelial cohesion, desmosomal junctions, and an intact basement membrane. In addition, we show that silencing of hepsin reduces invasive behavior of the mutant KRas harboring tumor xenografts. These findings expose serine protease hepsin as a critical upstream regulator of the Ras-dependent cancer degradome and point out hepsin as a potential therapeutic target for Ras pathway intervention strategies.

MATERIALS AND METHODS

See the **Supplementary Materials and Methods in the Supplementary data file** for **the ethical permits** (Table S1.)**, list of reagents** (Table S2.)**, antibodies** (Table S3)**, cell lines and culture media composition** (Table S4.)**, primer sequences** (Table S5.)**, shRNA sequences** (Table S6.) and **vector constructs** (Table S7.).

Human breast cancer samples and tissue from human reduction mammoplasties

Breast cancer specimens were derived from material sent to the pathology laboratory of the University of Helsinki Central Hospital in conjunction with elective surgery, and the set was previously published (30). The Helsinki University Hospital Ethics Committee approved the current study. License for the use of human breast cancer samples was granted by the National Supervisory Authority for Welfare and Health, and for the use of non-cancerous samples by the Ministry of Social Affairs and Health of Finland. Paraffin-embedded 5 μm thick sections of non-cancerous and breast cancer tumor tissue blocks were cut and plated onto objective glasses. Hepsin or phospho-ERK immunohistochemistry on sections was performed as described before (27,30). See Table S1. for complete information about ethical permits related to the use of human material in this study.

Genetically engineered mouse models

Experimental animal work was approved under a lisence (see Table S1) granted by The National Animal Ethics Committee of Finland. $Kras^{LSL}$-G12D (B6.129S4-$Kras^{tm4Tyj}$/J) (here Kras; C57Bl/6J background) and $Trp53^{fl/fl}$ mice (B6.129P2-*Trp53*^{tm1Brn}/J) (here p53; C57Bl/6J background) were crossed to produce Kras;p53 mouse line, a model for non-small cell lung cancer with advanced adenocarcinoma. To initiate tumor formation, mice were intranasally infected with adenovirus-CMV-Cre constructs (Gene Transfer Vector Core, University of Iowa, USA). After the mice were sacrificed, their lungs were fixed and processed for immunohistochemistry (IHC). See also SI Materials and Methods. For primary mouse mammary epithelial cell (MMEC) isolations and culturing see SI Materials and methods.

MDA-MB-231 xenografts

MDA-MB-231 breast cancer cells were transduced with recombinant lentiviral particles carrying shRNA hepsin, expanded, and validated for hepsin knockdown. Thereafter, 8 x 10^5 cells were transplanted subcutaneously in two to three sites on the back skin of NOD.CB17-*Prkdc*^{scid}/ J (NOD SCID) mice (a kind gift from Dr. Kari Alitalo, University of Helsinki). The end-point for tumor take rate and growth measurements was 33 days after the transplantation.

3D culture models

Briefly, human cell lines were 3D cultured in egg white whereas mouse primary mammary epithelial cells were embedded in Matrigel (Becton Dickinson). See SI Materials and Methods for details.

Cell culture and the cycloheximide (CHX) chase assay

Authenticated cell lines were obtained from ATCC (breast epithelial cell lines) or Invitrogen (293FT cells). MPE600 cell line was a gift from Dr. Outi Monni, University of Helsinki. Immediately upon arrival, cells were expanded and aliquoted into cell banks. The cell lines were cultured in +37°C and 5% CO_2 except for MDA-MB cell lines that were kept in +37°C and atmospheric air conditions. The cells were in general passaged twice per week with two media changes per week. The exact culture conditions are described in the Supplementary data. Our general laboratory practice allowed maximum of 30 passages per each vial thawed from the cell banks. All cell lines were regularly tested for mycoplasma contamination once every two months with MycoAlert PLUS detection kit (Lonza, cat# LT07-710) according to manufacturer's instructions. For CHX chase experiment, the cells were grown on petridishes until 80% confluent. Subsequently, the cells were treated with 50 μg ml^{-1} CHX (ready-made solution in DMSO, Merck) or DMSO control for indicated times in normal cell culture conditions. Cell lysates were collected as described below in the "Protein analysis" section.

Immunofluorescence staining (IF)

For 3D IF, the 3D cultures were fixed with 2% PFA, permeabilized with 100% methanol (-20°C) and blocked with 10% normal goat serum in IF buffer (0.1% BSA, 0.2% Triton-X, 0.05% Tween-20 in PBS). The structures were stained with primary antibodies, diluted in blocking buffer, overnight at 4°C. The structures were then washed in IF buffer and incubated for 45 min at RT with the appropriate Alexa Fluor secondary antibody diluted into the blocking buffer. For additional details and 2D methods see SI Materials and Methods.

Serine protease activity assays

To quantitate serine protease activity, the cells were treated with PBS (intact cells) or 1% Triton-X 100-PBS buffer (permeabilizing conditions) and, thereafter, fluorogenic tertbutoxycarbonyl-Gln-Arg-Arg-AMC (BOC-QRR-AMC) substrate was administered onto the cells. Peptide cleavage was measured at 37°C using an ELISA plate reader at wavelengths $350^{em}/450^{ex}$ nm. See SI Materials and Methods for other details.

Recombinant retroviruses

Retroviruses were produced in the Phoenix Ampho packaging cells (gift from Garry Nolan, Stanford University, Stanford, CA) by using total 2 μg of recombinant vector plasmid per 6-well plate well (5 x 10^5 cells seeded 24 h previously), and viral particles were collected after 72 h. Target cell transductions and recombinant lentivirus production were performed as described before (31).

Immunoblot and Immunoprecipitation analyses

For protein extraction, the cells were lysed on ice using 1% Triton-X 100 with or without phosphatase inhibitors. Immunoblotting was performed as described in (30). Quantitation of loading normalized band intensity of at least three biological replicates was performed with ImageJ software (Version: 2.0.0-rc-69/1.52n, RRID:SCR_003070). For those experiments not quantitated, a representative western blot results exemplary of at least three biological replicates is shown. For immunoprecipitation assays, the cell lysates were

prepared as above. Immunoprecipitation was performed with Dynabeads™ Protein G (Invitrogen/Thermo Fisher Scientific) system according to the manufacturer's instructions.

qRT-PCR, cloning, transfections, image acquisition, image analysis and quantitation. The methods have described in SI Materials and Methods.

RESULTS

Oncogenic Ras induces expression and proteolytic activity of hepsin

Hepsin protease activity has been commonly interpreted through proxies, which include elevated expression, processing of hepsin to its active 31 kDa fragment, or a redistributed hepsin expression pattern. We found in an earlier study that ectopic expression of hepsin associates with rapid downmodulation of hepsin's cognate inhibitor hepatocyte growth factor activator inhibitor-1 (HAI-1)(27), which prompted us to determine whether the normalized hepsin-HAI-1 (h-H) ratio offers a more sensitive proxy for hepsin activity than processed hepsin levels alone. We used MCF10A-hepsin^{IND20} cells expressing doxycycline (DOX)-inducible hepsin (27) to compare non-induced (endogenous hepsin) and DOX-induced states, and found that the h-H ratio yields an improved sensitivity (11-fold) in comparison to the analysis of the 31 kDa hepsin fragment alone (1.6-fold) (Fig. 1a).

Next, we analyzed the h-H ratio in MCF10A cells engineered to express common oncogenic proteins (Fig. 1b and Supplementary Fig. 1a, b**)** and found that oncogenic HRas^{V12}, and to a lesser extent E2F-1, prominently increases the h-H ratio (Fig. 1b and Supplementary Fig. 1c). In addition to HRas^{V12}, also KRas^{V12} and ectopic wild-type KRas increased the h-H ratio (Fig. 1c and Supplementary Fig. 1d and e). In addition to MCF10As, HRas^{V12} also augmented the h-H ratio when stably expressed in two other non-malignant breast epithelial cell lines (Fig. 1d and Supplementary Fig. 1f and g). HRas^{V12} also enhanced the total proteolytic activity of hepsin, supported by evidence of enhanced cleavage of the preferred hepsin peptide substrate BOC-QRR-AMC in both intact and permeabilized MCF10A cells (Fig. 1e, f, see also Fig. 1a).

Ras and PI3K pathway mutations are mutually exclusive in breast cancer (32), which led us to explore the h-H ratio in a panel of seven genetically profiled breast cancer cell lines (33); three of which harboring an activating *PIK3CA* mutation but wild-type *HRAS* and *KRAS* alleles (PIK3CAmut cells) and three others harboring activating mutations in *HRAS* or *KRAS* but wild-type *PIK3CA* and *PTEN* (Ras mut cells). One cell line with an

inactivating *RB1* mutation (RB1 mut cells) was examined, since deficiency in RB1 unleashes E2F proteins (33).

We measured a high (>10) h-H ratio in MCF10A-HRas^{V12} cells (positive control), in two out of the three Ras mut breast cancer cell lines and in the RB1 mut cells (Fig. 1g and Supplementary Fig. 1h). On the contrary, the h-H ratio was low (<1) in all PI3KCAmut cell lines. Furthermore, introduction of an ectopic wild-type KRas into the T47D PIK3CAmut cell line with low baseline h-H ratio increased the level of 31 kDa hepsin and decreased HAI-1, thus substantially increasing the h-H ratio (Fig. 1h and Supplementary Fig. 1i, see also Fig. 1g). Taken together, oncogenic Ras proteins strongly upregulate hepsin protein expression and enhance its proteolytic activity in non-transformed and cancerous cells.

Oncogenic Ras extends the half-life of hepsin protein

The effect of HRas^{V12} on h-H ratio was observed in all studied non-transformed mammary epithelial cell lines and in the majority of Ras mutant breast cancer cell lines (Fig. 1b-d, g, h and Supplementary Fig. 1c-i). However, the oncogenic Ras proteins did not alter hepsin mRNA levels (Fig. 2a), suggesting altered translation or protein stability. In support of enhanced stability, HRas^{V12} extended the half-life of hepsin in conditions where new protein translation was blocked with cycloheximide (Fig. 2b, and Supplementary Fig. 1j).

Ubiquitin tagging is a common denominator in the targeting of proteins to all three major protein degradation pathways in mammalian cells: the proteasome, the lysosome, and the autophagosome (34). Consistent with the notion that oncogenic Ras reduces hepsin turnover, we found that KRas^{V12} expression reduces steady state hepsin ubiquitination (Fig 2c, quantitation: Supplementary Fig. 1k). To define the major cellular degradation pathway for hepsin, we inhibited proteasome-mediated degradation pathways with three different compounds in three mammary epithelial cell lines with low or intermediate hepsin protein expression (MCF10A, T47D and MCF7). However, proteasome inhibition did not affect hepsin turnover (Supplementary Fig. 1l). In contrast, inhibition of the lysosomes with bafilomycin B1 or concanamycin A led to a clear accumulation of hepsin protein in all cell

lines tested (Fig. 2d). We also found that hepsin co-localizes with the lysosomal protein lamp2 (Fig. 2e). The co-localization was observed in untreated cells and most visibly in the cells treated with bafilomycin B1. These results suggest that the hepsin turnover is predominantly regulated by the lysosomal pathway.

To define the impact of $HRas^{V12}$ on the lysosomal localization of hepsin, we quantitated the co-localization pattern of hepsin and lamp 2 in MCF10A-HRasV12 cells (Fig. 2e). While the total co-localization (co-localized pixel value per cell) was increased (Fig. 2e), the lysosome-size normalized co-localization of hepsin and lamp2 was decreased in MCF10A-HRasV12 cells as compared to the control MCF10A cells (Fig. 2f). We also analyzed the total lysosomal activity in $HRas^{V12}$ expressing cells, finding that the total lysosomal activity is increased by Ras (Supplementary Fig. 1m). These observations are consistent with the earlier studies on the lysosomal effects of Ras (35,36). Thus, we conclude that $HRas^{V12}$ expressing cells have active lysosomes able to import hepsin but we also note that $HRas^{V12}$ may slightly reduce the lysosomal import of hepsin. This finding is congruent with the notion that $HRas^{V12}$ reduces the steady state ubiquitylation of hepsin

The Ras-MAPK-HSF1 pathway upregulates hepsin

We generated MCF10A cells expressing a doxycycline (DOX)-inducible $HRas^{V12}$ to explore the acute effects of $HRas^{V12}$ on hepsin and HAI-1 (Supplementary Fig. 2a). In MCF10A-Ind20-$HRas^{V12}$ cells, DOX induction of $HRas^{V12}$ elevated the levels of active 31 kDa hepsin fragment and enhanced the proteolytic QRRase activity within 48 h without affecting hepsin mRNA levels (Supplementary Fig. 2b). Furthermore, long-term (24 d) induction of $HRas^{V12}$ persistently upregulated the 31 kDa active hepsin (Fig. 3a). The level of DOX induction of hepsin ($hepsin^{Ind20}$+DOX, see Fig. 1a) was about 1.6-fold over the control and the level of hepsin expression induced by $HRas^{V12}$ (Ind20-$HRas^{V12}$ +DOX) was in average 2.8-fold over the control (Fig. 3a). Surprisingly, a long term $HRas^{V12}$ induction was required for downregulation of HAI-1 levels, suggesting that $HRas^{V12}$ regulates hepsin and HAI-1 via separate signaling mechanisms rather than hepsin being directly causal to HAI-1 downmodulation (Fig. 3a, b). Hepsin can directly downregulate HAI-1 via a shedding mechanism (27), but it appears that $HRas^{V12}$ regulates the balance of

hepsin and HAI-1 in a more complex manner. We did not follow up further the mechanisms of HAI-1 downmodulation, instead we sought more insight into the mechanisms whereby $HRas^{V12}$ regulates hepsin protein stability.

GTP bound Ras recruits more than seven distinct Ras effector pathways for signaling, including the Raf-MEK-ERK mitogen-activated protein kinase (MAPK) cascade, phosphoinositide 3-kinase (PI3K)– AKT-mTOR and the RalGEF-Ral small GTPase signaling networks (37). We examined which $HRas^{V12}$ pathways are responsible for hepsin upregulation by using seven small molecule inhibitors targeting either the MAPK or PI3K pathways (Fig. 3c). The experiments revealed that only inhibition of MEK or ERK suppresses the $HRas^{V12}$-induced upregulation of hepsin and its proteolytic activity (Fig. 3d-h and Supplementary Fig. 2c).

The Ras-MAPK pathway is classically pictured as a kinase signaling cascade, which results in translocation of a pool of ERK molecules to the nucleus (38). Nuclear ERK targets multiple transcription factors, including ELK1 and c-MYC, followed by transcriptional induction of mitogen-induced gene sets (39). While none of the classical MAPK-associated functions provided tangible rationale to explain hepsin stabilization, we were intrigued by recent findings linking Ras-MAPK signaling to MEK-induced phosphorylation of HSF1 (40). HSF1 is a stress-sensing transcription factor, which induces expression of heat shock proteins that act as molecular chaperones to counteract protein misfolding and proteotoxicity (41). Notably, MEK-HSF1 targets include many plasma membrane receptors and proteins (40). We observed that both constitutive and inducible $HRas^{V12}$ upregulate the HSF1 protein expression and induce HSF1 phosphorylation at its activating residue Ser326 (Fig. 3i and Supplementary Fig. 2d). This HSF1 activation was inhibited by MEK or ERK inhibitor, indicating MAPK pathway as a mediator (Supplementary Fig. 2e). In addition, ectopic co-expression of hepsin and HSF1 increased hepsin levels, which shows that HSF1 can regulate hepsin turnover (Fig. 3j and Supplementary Fig. 2f). In vertebrates, heat-shock induces HSF1 activation, and HSF1 together with other heat shock transcription factors coordinate the upregulation of heat-shock genes (42). We used heat-shock as a physiological stimulus to activate endogenous HSF1, finding that heat-shock

leads to accumulation of hepsin concomitantly with S326 phosphorylated HSF1 (Fig. 3k). This heat shock induction of hepsin was blocked by KRIBB11, a small molecule inhibitor that interferes with HSF1's transcription factor function (Fig. 3k) (43). We also silenced HSF1 by shRNA, finding that loss of HSF1 downmodulates hepsin protein levels in all tested cells expressing either ectopically or endogenously mutant Ras (Fig. 3l, m, Supplementary Fig. 2g-i). Finally, we silenced HSF1 by shRNA in cells that were engineered to transiently overexpress hepsin and $KRas^{V12}$. We observed that the mutant Ras-induced diminished hepsin ubiquitination was rescued by loss of HSF1 (Fig. 3n and Supplementary Fig. 2j, see also Fig. 2c). These findings demonstrate that the mechanisms whereby Ras-MAPK stabilize hepsin include HSF1 stress signaling pathway, which can regulate protein turnover via enhanced chaperoning activity through the action of heat shock proteins (Supplementary Fig. 2k).

Oncogenic Ras disrupts hepsin-enriched epithelial junctions and induces desmosomes-to-cytosol redistribution of hepsin

In the normal human breast tissue samples obtained via reduction mammoplasty, hepsin expression is strictly restricted to the basal and basolateral sides of the alveolar epithelial cells (Fig. 4a) (27), which contrasts to breast tumor samples where hepsin is typically redistributed to the cytoplasm (27,28,44). In agreement, examination of a panel of 49 breast cancer samples showed strong hepsin immunoreactivity in as many as 41 samples (84%) (upper histogram) and the staining pattern was diffuse in >70% of the samples (lower histogram) (Fig. 4a**)**.

Earlier studies have exposed hepsin colocalization with both desmosomal and hemidesmosomal proteins in non-transformed cells and some cancer cell types (26,27). Desmosomes (DM) and hemidesmosomes (HDM) are both anchoring junctions that stabilize intercellular and cell-BM adhesions, respectively. Interestingly, similar to tumor samples, the Ras mut and RB1 mut TNBC cell lines all showed diffuse cytoplasmic hepsin staining in monolayer 2D cultures. These cell lines lacked pericellular desmoplakin, indicating loss of DMs (Fig. 4b and Supplementary Fig. 3a). In contrast to mutant Ras expressing cells, hepsin was expressed in the pericellular or pericellular/cytoplasmic

regions in PIK3CAmut cells with strong overall colocalization with desmoplakin (Fig. 4b and Supplementary Fig. 3a). The proteolytic activity of hepsin corresponding to the cell lines shown in Fig. 4b is shown on the right side of the images (Fig. 4b). These results show a correlation between the oncogenic Ras activity and desmosomes-to-cytosol redistribution of hepsin in breast cancer cells. Furthermore, we found that introduction of ectopic oncogenic $HRas^{V12}$ into non-transformed mammary epithelial cells (MCF10A, MCF12A and HMEC-hT) induced desmosomes-to-cytosol redistribution of hepsin, resembling the expression pattern observed in the mutant Ras expressing breast cancer cell lines (Fig. 4c, and Supplementary Fig. 3b). Ectopic $HRas^{V12}$, $KRas^{V12}$ and wild type KRas all resulted in similar impact on hepsin in isogenic MCF10A background (Fig. 4c, d). Moreover, all Ras-transformed cells consistently showed loss of pericellular desmoplakin (Fig. 4c, d).

Oncogenic Ras dissolves the hepsin-enriched basement membrane

In three-dimensional (3D) MCF10A cultures epithelial cells form normal breast alveolus-like structures. In these cultures, hepsin localizes predominantly to BM as it does in the alveoli of normal human breast (Fig. 4a). Previous (27) and current immunofluorescence (IF) studies indicate colocalization of hepsin with the HDM markers laminin 332 and α6 integrin in the non-transformed mammary epithelial 3D cultures (Supplementary Fig. 3c). The analysis of the breast cancer cell lines, which were able to form 3D structures in the egg white matrix (see below for rationale), showed that the PIK3CAmut cell lines MCF-7 and T47D formed alveolus-like structures with basolateral hepsin expression (Fig. 4e). The Ras mut cell lines Hs578T, MDA-MB-231 and MDA-MB-436 formed much less cohesive structures with cytosolic staining of hepsin. When MCF10A cultures with or without oncogenic Ras were compared, the controls showed basolateral expression of hepsin whereas the $HRas^{V12}$ or $KRas^{V12}$ transformed structures showed cytosolic hepsin in poorly cohesive 3D structures (Fig. 4e). We also compared the effects of two classical co-operating oncogenes MYC and $HRas^{V12}$, finding that only $HRas^{V12}$ induced cytoplasmic redistribution of hepsin and loss of cohesion in 3D structures (Fig. 4f, note the loss of HDM markers laminin-332 and α6-integrin, Supplementary Fig. 3d). Immunoblot analysis of MCF10A-$HRas^{V12}$ lysates showed cleavage of the laminin-332 ß3 chain (Fig. 4g), which

is a demonstrated proteolytic target of hepsin (27,45). Notably, we used egg white matrix in all 3D experiments since this matrix does not contain matrix-derived BM components (like laminin-rich Matrigel) and is therefore expectedly more sensitive scaffold for analysis of invasive potential than artificially reconstituted basement membrane gels (46). All basal BM comes from the cells that form epithelial structure in the egg white based 3D cultures (27). Specifically, in the egg white cultured $HRas^{V12}$ transformed structures, the dissolution of BM correlated with diminished overall cohesion and occasional detachment of the cells from colonies, which phenotypes are reminiscent of the early invasive processes observed in vivo (Fig. 4f).

Impact of endogenous $Kras^{G12D}$ on hepsin

To determine whether the endogenous levels of oncogenic Ras upregulate hepsin and induce its redistribution, we investigated mammary epithelial cells freshly isolated from mice harboring a conditional Lox-Stop-Lox (LSL)-$Kras^{G12D}$ allele (47). The expression of $Kras^{G12D}$ was induced *ex vivo* by infecting the isolated cells with Cre-expressing adenoviruses (AdCre), and subsequently, the cells were cultured in 3D (Supplementary Fig. 4a). Similar to the effects observed in MCF10A-$HRas^{V12}$ culture experiments in Fig. 4f, also endogenous active $Kras^{G12D}$ promoted development of abnormally large and misshapen epithelial 3D structures, increased 31 kDa hepsin expression level (in 5 out of 7 mammary epithelial cell preparations isolated from different mice) and induced redistribution of hepsin from basolateral membranes to the cytosol (Fig. 4h and i, and Supplementary Fig. 4a-c). Closer inspection revealed individual cells bulging out from the cultured 3D structures (Supplementary Fig. 4d). Next, we examined whether the physiological expression level of $Kras^{G12D}$ induces redistribution of hepsin *in vivo*. $Kras^{G12D}$ was induced in a p53 null background by nasal inhalation of AdCre, which leads to formation of focal lung adenocarcinomas (48,49). About 65% of the tumors manifested strong cytosolic hepsin immunostaining, contrasting to weak or absent hepsin expression in healthy lungs (Fig. 4j and Supplementary Fig. 4e). Thus, both the ectopic and endogenous expression of oncogenic Ras induces cytosolic redistribution and upregulation of 31kDa active hepsin concomitantly with compromised epithelial integrity, dissolution of BM and cellular bulging phenotype never observed in the control epithelial structures.

Ras effects on subcellular expression pattern of hepsin is mediated via the MAPK pathway

Since the Ras-induced biochemical effects such as stabilization and proteolytic activity of hepsin were mediated via MAPK pathway (Fig. 3d, e, h, and Supplementary Fig. 2c), we asked whether MAPK pathway is also involved in mediating the subcellular redistribution of hepsin. Indeed, MEK or ERK inhibition fully prevented Ras from inducing hepsin mislocalization and these inhibitors restored the desmosomal expression pattern of hepsin (Fig. 5a). In the 3D cultures of MCF10A-HRas^{V12} cells, MEK and ERK inhibitors restored the symmetric morphology, basal expression pattern of hepsin, as well as colocalization of laminin-332 and α6-integrin at the BM (Fig. 5b). Thus, intervention of the oncogenic Ras pathway via the inhibitors of MAPK pathway fully restores the normal expression pattern and activity of hepsin.

Ras mutations are rare in breast cancer, but a number of other mechanisms eliciting overactive Ras-MAPK signaling have been reported in breast cancer - for example Ras gene amplification, overexpression of EGF, HER2 and other receptor tyrosine kinases, and loss of pathway inhibition via mutated RAS GAPs (7,9-11,50)(Supplementary Fig. 5a). To determine whether overactive MAPK pathway associates with high levels of hepsin in breast cancer, we determined the hepsin and phospho-ERK (pERK) expression in serial sections cut from paraffin embedded tumor samples corresponding to 57 breast cancer patients (Supplementary Fig. 5b) (30). We found that about 80% of the breast cancer samples showed intense pERK staining and two-thirds (66%) of the samples were double positive for pERK and hepsin (hepsin^{high}/pERK^{high}) (Fig. 5c).

Hepsin is required for the Ras-induced loss of epithelial integrity

To explore the role of hepsin in Ras-mediated disruption of epithelial cohesion, we silenced hepsin by an shRNA approach in MCF10A-HRas^{V12} cells. Knockdown of hepsin diminished hepsin activity and restored HAI-1 expression (Fig. 6a, b and Supplementary Fig. 5c). In 2D Petri dish cultures of MCF10A-HRas^{V12} cells, the hepsin knockdown partially rescued desmosomes and the residual low levels of hepsin, that escaped

knockdown, predominantly co-localized with desmoplakin in the pericellular regions (Fig. 6c). In 3D cultures of MCF10A-HRas^{V12} cells, hepsin knockdown had a dramatic effect both on morphology and HDMs; hepsin shRNAs robustly rescued the symmetrical glandular morphology of the HRas^{V12}-transformed structures and restored the basal expression of α6-integrin and the ß3 and γ2 chains of laminin-332 (Fig. 6d). Moreover, silencing of hepsin inhibited the proteolytic processing of laminin 332 ß3, which occurred in control MCF10A-HRas^{V12} cells (Fig. 6e). In 3D culture, HRas^{V12} expression perturbed apical polarity, as indicated by disorientation of the apical Golgi marker GM130, but this apical polarity defect could not be rescued by knockdown of hepsin (Fig. 6f).

To confirm the results suggesting a critical role for hepsin as a mediator of the loss of epithelial cohesion caused by oncogenic Ras, we employed a hepsin neutralizing antibody (Ab25) for the experiments (51,52). The MCF10A-Ind20-HRas^{V12} cells were cultured for four days in an exogenous basement membrane-free egg white hydrogel to form acinar structures, followed by three day DOX treatment to acutely induce HRas^{V12}. The DOX-induced HRas^{V12} expression, like chronic HRas^{V12} expression, resulted in a disruption of epithelial integrity and loss of HDMs (Fig. 6g). These effects were fully prevented by the hepsin function blocking antibody Ab25 that inhibited peptide cleavage activity in 3D as well (Fig. 6g, Supplementary Fig. 5d). Together, these findings indicate a key role for hepsin as a mediator of Ras-dependent disruption of the epithelial integrity, involving loss of adhesive DM and HDM structures.

Silencing of hepsin reduces tumor take rate and invasive growth of KRas^{G13D} MDA-MB-231 xenografts

We examined the role of hepsin in tumor growth using an MDA-MB-231 xenograft model of triple-negative breast cancer. Hepsin was silenced by shRNA in the MDA-MB-231 breast cancer cells, which carry a mutant KRas; KRas^{G13D} (cBioportal). After validation of hepsin knockdown, the cells were subcutaneously transplanted to the host mice. We observed a lower take rate for the cells transduced with shRNA for hepsin (Fig. 7a). In addition, tumor growth was somewhat slower in the groups with silenced hepsin although the results did not reach statistical significance (Fig. 7b). We investigated the local tumor

invasion pattern from formalin fixed sections subjected to hematoxylin and collagen IV staining and found that the tumor growth pattern was clearly different between the tumors originating from control or hepsin shRNA transduced cells. The control samples typically showed a tight tumor bulk (T) predominantly composed of tumor cells and a surrounding region showing a mixture of tumor cells and muscle cells (T/M) or tumor cells and fat cells (T/F) (Fig. 7c). Those areas showing a mixture of cells represented the invasive tumor front (ITF). The ITF was significantly smaller in tumors originating from shHepsin #1 or #5 transduced MDA-MB-231 cells in comparison to the controls (Fig. 7c). We also analyzed the expression pattern of collagen IV, which is a major basement membrane component, finding that loss of hepsin led to a significant increase in the collagen IV levels within the tumor tissue (Fig. 7d). These results suggest an important role for hepsin in the establishment of invasive front by the TNBC cells of tumor grafts.

Together, our findings suggest a previously unanticipated functional role for the type II transmembrane serine protease hepsin as a component of the oncogenic Ras pathway (Fig. 7e). The Ras-MAPK-HSF1 pathway enhances hepsin activity to disrupt junctional integrity, basement membrane and epithelial cohesion, which are cellular events that commonly associate with the earliest stages of tumor invasion.

DISCUSSION

In this study, we show that oncogenic Ras proteins upregulate the expression and activity of the transmembrane serine protease hepsin via a set of molecular events that act downstream of the Ras-MEK-ERK pathway. In the context of Ras transformed epithelial tissue, dysregulated hepsin has a crucial role in mediating disruption of epithelial integrity that involves loss of desmosomal structures important for cell-cell adhesion and loss of hemidesmosomal structures important for cell-basement membrane adhesion.

Earlier studies have proposed that the functional changes observed in cancer cell proteomes, which ultimately lead to enhanced enzyme activity, are commonly due to altered posttranscriptional and posttranslational mechanisms rather than transcriptional changes (53,54). Here, we show evidence that Ras stabilizes hepsin and upregulates its proteolytic activity through the MEK-HSF1 stress signaling pathway. The MEK pathway has been previously shown to upregulate HSF1 via MEK-dependent phosphorylation of HSF1 at S326 and upregulated HSF1 affects the stability of number of proteins via heat shock proteins (40). For example, in response to acute stress, HSF1 transcriptionally induces the expression of HSP27 that augments the basal chaperoning activity provided by non-inducible HSC70 and HSP90 proteins (55). The HSF1 response is normally transient due to negative feedback loops, but in cancer is often constitutively active (55). We found that HSF1 is required for hepsin upregulation in the presence of active Ras signaling and that in the absence of oncogenic Ras, both the ectopic HSF1 expression and heat shock treatment via HSF1 is sufficient to upregulate the protein levels of hepsin.

We also demonstrated that oncogenic Ras decreases the steady state ubiquitination of hepsin and that this effect was mediated via HSF1. Ubiquitin tagging can target proteins to all three major protein degradation pathways in mammalian cells: the proteasome, the lysosome, and the autophagosome (34) and our experiments suggest that the turnover of hepsin is primarily regulated by the lysosomal degradation pathway. These results, altogether, would be consistent with a model that Ras-MEK-HSF1 pathway reduces the steady state ubiquitination of hepsin, which then inhibits transit of hepsin from the

membranes via endosomes to the lysosomes. Indeed, for many transmembrane receptors, ubiquitination is a signal that triggers endocytosis and transport to the lysosome for degradation (56). However, while $HRas^{V12}$ transformed cells showed proportionally less hepsin in their lysosomes than control cells, the difference was small, and the lysosomes were highly active in the $HRas^{V12}$ transformed cells. Therefore, the "suppressed lysosomal transport" model is at this stage still only speculative and requires further investigations. The alternative possibility, also supported by the current data, is that hepsin is accumulated outside the lysosomal compartment due to enhanced chaperoning activity instated by oncogenic Ras-HSF1 pathway (Supplementary Fig. 2k). In this model, stabilization of hepsin is part of the adaptive cellular response to Ras-induced chronic oncogenic stress. While the natural stress response primarily occurs to alleviate proteotoxic stress in circumstances of acute stress signaling, chronic oncogenic stress may lead to a number of hazardous pro-tumorigenic events such as dysregulated expression and activity of hepsin. While the exact mechanisms coupling HSF1 to upregulation of hepsin remain to be clarified, the current study clearly adds hepsin to a list of pro-tumorigenic proteins upregulated by the MAPK-HSF1 stress branch of Ras signaling.

In both normal breast epithelium and mammary epithelial 3D culture, hepsin most visibly localizes to the BM and basolateral membranes. More specifically, data from the present and earlier studies have shown that in the basolateral membranes hepsin colocalizes with lateral DM proteins and with HDM in the basement membrane (26,27,30). Strikingly, in Ras-transformed 3D cultures, which show loss of epithelial integrity and severe loss of HDM, the inhibition of hepsin by shRNA or with a function-blocking antibody nearly completely rescued basal α6-integrin and laminin-332 expression, as well as the BM integrity. The apical polarity marker GM130 was not rescued, whereas DM which overlap with the site of hepsin expression were also rescued in HRas-transformed cultures. It remains somewhat an open question whether Ras upregulates the hepsin activity first, and then this event is causal to loss of DM, HDM and epithelial integrity. Alternatively, Ras could activate hepsin and induce its redistribution more indirectly - by disrupting junctional protein complexes that normally determine the spatial localization of hepsin. However, in this latter case hepsin inhibition might not have such dramatic epithelial integrity

normalizing actions as we show in the present study. In support of the "hepsin first" model, earlier findings have shown that ectopic doxycycline-induced overexpression and enhanced activity of hepsin alone induces similar deteriorating effects on DM and HDM as we show here with Ras (27). It should be noted, however, that even if hepsin is crucially important for the Ras-induced loss of epithelial cohesion, it is unlikely that hepsin performs all epithelial cohesion eroding activities alone. For example, earlier studies have implicated a role for matrix metalloproteinase-9 (MMP-9) as a downstream mediator of Ras in those events that disrupt polarity, the laminin-111 component of the basement membrane, and epithelial integrity in 3D culture (21). Moreover, hepsin has been linked to activation of pro-matrix metalloproteinases in osteoarthritis and prostate cancer models (57,58).

Collectively, our findings suggest that overactive hepsin is an integral part of the Ras-dependent degradome, promoting the loss of desmosomal and hemidesmosomal junction integrity, and contributing to the loss of basement membrane structure and overall epithelial integrity. Such proteolytic events contribute to processes that provide tumor cells invasive potential. In support of a role for hepsin in local tumor invasion, we found that ablation of hepsin in KRas mutant MDA-MB-231 cells generated tumor with diminished invasive potential. Hepsin-deficient tumors displayed increased deposition of collagen IV, which is a major component of basement membrane. These results are consistent with the proposed role of hepsin in regulation of the basement membrane homeostasis. We believe that hepsin as an extracellular and hence drug or antibody-accessible protease could offer an attractive target for future anticancer drug development aiming to target not only dysfunctional cell proliferation machinery but also early stages of tumor dissemination.

AUTHORS' CONTRIBUTIONS

T.A.T. designed the study, provided reagents, performed experiments, provided and analyzed the data, and wrote the manuscript. J.K. designed the study, provided and analyzed the data, and wrote the manuscript. J.E. designed the study, provided reagents, performed experiments, provided and analyzed the data. S.M.P., D.B. and K.N. performed experiments, provided and analyzed the data. E.W.V. designed the study, provided

reagents and edited the manuscript. C.H. provided reagents. P.K. provided reagents, helped with analysis, clinical data, and patient samples.

ACKNOWLEDGEMENTS

We are grateful to Biomedicum Functional Genomics Unit/Libraries (FuGU/Libraries), Biomedicum Virus Core Unit (BVC), Genome Biology Unit (GBU) and Biomedicum Imaging Unit (BIU), and Laboratory Animal Center (LAC) (all from HiLIFE, University of Helsinki and Biocenter Finland) for their services. We thank Dr. Jeroen Pouwels and other Klefström laboratory personnel for discussions and critical comments on the manuscript. We thank for technical assistance provided by T. Raatikainen, M. Merisalo-Soikkeli, K. Karjalainan and T.Välimäki. This work was funded by grants from The Academy of Finland, Business Finland, EU H2020 RESCUER, Finnish Cancer Organizations, Sigrid Juselius Foundation and iCAN Digital Precision Cancer Medicine Flagship. T.A.T. was funded by the Helsinki Institute of Life Science Infrastructures (HiLIFE) of University of Helsinki.

REFERENCES

1. Friedl P, Alexander S. Cancer invasion and the microenvironment: plasticity and reciprocity. Cell 2011;147:992-1009.
2. Gonzalez-Rodriguez D, Guevorkian K, Douezan S, Brochard-Wyart F. Soft matter models of developing tissues and tumors. Science 2012;338:910-7.
3. Padmanaban V, Krol I, Suhail Y, Szczerba BM, Aceto N, Bader JS, et al. E-cadherin is required for metastasis in multiple models of breast cancer. Nature 2019;573:439-44.
4. Sevenich L, Joyce JA. Pericellular proteolysis in cancer. Genes Dev 2014;28:2331-47.
5. Khan AQ, Kuttikrishnan S, Siveen KS, Prabhu KS, Shanmugakonar M, Al-Naemi HA, et al. RAS-mediated oncogenic signaling pathways in human malignancies. Semin Cancer Biol 2019;54:1-13.
6. Zhou B, Der CJ, Cox AD. The role of wild type RAS isoforms in cancer. Semin Cell Dev Biol 2016;58:60-9.
7. Cancer Genome Atlas N. Comprehensive molecular portraits of human breast tumours. Nature 2012;490:61-70.
8. von Lintig FC, Dreilinger AD, Varki NM, Wallace AM, Casteel DE, Boss GR. Ras activation in human breast cancer. Breast Cancer Res Treat 2000;62:51-62.
9. Razavi P, Chang MT, Xu G, Bandlamudi C, Ross DS, Vasan N, et al. The Genomic Landscape of Endocrine-Resistant Advanced Breast Cancers. Cancer Cell 2018;34:427-38 e6.
10. Giltnane JM, Balko JM. Rationale for targeting the Ras/MAPK pathway in triple-negative breast cancer. Discov Med 2014;17:275-83.
11. Olsen SN, Wronski A, Castano Z, Dake B, Malone C, De Raedt T, et al. Loss of RasGAP Tumor Suppressors Underlies the Aggressive Nature of Luminal B Breast Cancers. Cancer Discov 2017;7:202-17.
12. Galie M. RAS as Supporting Actor in Breast Cancer. Front Oncol 2019;9:1199.
13. Land H, Parada LF, Weinberg RA. Tumorigenic conversion of primary embryo fibroblasts requires at least two cooperating oncogenes. Nature 1983;304:596-602.
14. Mercer JA. Intercellular junctions: downstream and upstream of Ras? Semin Cell Dev Biol 2000;11:309-14.
15. Potempa S, Ridley AJ. Activation of both MAP kinase and phosphatidylinositide 3-kinase by Ras is required for hepatocyte growth factor/scatter factor-induced adherens junction disassembly. Mol Biol Cell 1998;9:2185-200.
16. Chen Y, Lu Q, Schneeberger EE, Goodenough DA. Restoration of tight junction structure and barrier function by down-regulation of the mitogen-activated protein kinase pathway in ras-transformed Madin-Darby canine kidney cells. Mol Biol Cell 2000;11:849-62.
17. Edme N, Downward J, Thiery JP, Boyer B. Ras induces NBT-II epithelial cell scattering through the coordinate activities of Rac and MAPK pathways. J Cell Sci 2002;115:2591-601.
18. Magudia K, Lahoz A, Hall A. K-Ras and B-Raf oncogenes inhibit colon epithelial polarity establishment through up-regulation of c-myc. J Cell Biol 2012;198:185-94.

19. Liu JS, Farlow JT, Paulson AK, Labarge MA, Gartner ZJ. Programmed cell-to-cell variability in Ras activity triggers emergent behaviors during mammary epithelial morphogenesis. Cell Rep 2012;2:1461-70.
20. Pearson GW, Hunter T. Real-time imaging reveals that noninvasive mammary epithelial acini can contain motile cells. J Cell Biol 2007;179:1555-67.
21. Beliveau A, Mott JD, Lo A, Chen EI, Koller AA, Yaswen P, et al. Raf-induced MMP9 disrupts tissue architecture of human breast cells in three-dimensional culture and is necessary for tumor growth in vivo. Genes Dev 2010;24:2800-11.
22. Hernandez-Alcoceba R, del Peso L, Lacal JC. The Ras family of GTPases in cancer cell invasion. Cell Mol Life Sci 2000;57:65-76.
23. Campbell PM, Der CJ. Oncogenic Ras and its role in tumor cell invasion and metastasis. Semin Cancer Biol 2004;14:105-14.
24. Szabo R, Bugge TH. Type II transmembrane serine proteases in development and disease. Int J Biochem Cell Biol 2008;40:1297-316.
25. Matsuo T, Nakamura K, Takamoto N, Kodama J, Hongo A, Abrzua F, et al. Expression of the serine protease hepsin and clinical outcome of human endometrial cancer. Anticancer Res 2008;28:159-64.
26. Miao J, Mu D, Ergel B, Singavarapu R, Duan Z, Powers S, et al. Hepsin colocalizes with desmosomes and induces progression of ovarian cancer in a mouse model. Int J Cancer 2008;123:2041-7.
27. Tervonen TA, Belitskin D, Pant SM, Englund JI, Marques E, Ala-Hongisto H, et al. Deregulated hepsin protease activity confers oncogenicity by concomitantly augmenting HGF/MET signalling and disrupting epithelial cohesion. Oncogene 2016;35:1832-46.
28. Xing P, Li JG, Jin F, Zhao TT, Liu Q, Dong HT, et al. Clinical and biological significance of hepsin overexpression in breast cancer. J Investig Med 2011;59:803-10.
29. Betsunoh H, Mukai S, Akiyama Y, Fukushima T, Minamiguchi N, Hasui Y, et al. Clinical relevance of hepsin and hepatocyte growth factor activator inhibitor type 2 expression in renal cell carcinoma. Cancer Sci 2007;98:491-8.
30. Partanen JI, Tervonen TA, Myllynen M, Lind E, Imai M, Katajisto P, et al. Tumor suppressor function of Liver kinase B1 (Lkb1) is linked to regulation of epithelial integrity. Proc Natl Acad Sci U S A 2012;109:E388-97.
31. Partanen JI, Nieminen AI, Makela TP, Klefstrom J. Suppression of oncogenic properties of c-Myc by LKB1-controlled epithelial organization. Proc Natl Acad Sci U S A 2007;104:14694-9.
32. Castellano E, Downward J. RAS Interaction with PI3K: More Than Just Another Effector Pathway. Genes Cancer 2011;2:261-74.
33. Hollestelle A, Nagel JH, Smid M, Lam S, Elstrodt F, Wasielewski M, et al. Distinct gene mutation profiles among luminal-type and basal-type breast cancer cell lines. Breast Cancer Res Treat 2010;121:53-64.
34. Clague MJ, Urbe S. Ubiquitin: same molecule, different degradation pathways. Cell 2010;143:682-5.
35. Collette J, Ulku AS, Der CJ, Jones A, Erickson AH. Enhanced cathepsin L expression is mediated by different Ras effector pathways in fibroblasts and epithelial cells. Int J Cancer 2004;112:190-9.

36. Urbanelli L, Trivelli F, Ercolani L, Sementino E, Magini A, Tancini B, et al. Cathepsin L increased level upon Ras mutants expression: the role of p38 and p44/42 MAPK signaling pathways. Mol Cell Biochem 2010;343:49-57.
37. Simanshu DK, Nissley DV, McCormick F. RAS Proteins and Their Regulators in Human Disease. Cell 2017;170:17-33.
38. Kolch W. Coordinating ERK/MAPK signalling through scaffolds and inhibitors. Nat Rev Mol Cell Biol 2005;6:827-37.
39. Wortzel I, Seger R. The ERK Cascade: Distinct Functions within Various Subcellular Organelles. Genes Cancer 2011;2:195-209.
40. Tang Z, Dai S, He Y, Doty RA, Shultz LD, Sampson SB, et al. MEK guards proteome stability and inhibits tumor-suppressive amyloidogenesis via HSF1. Cell 2015;160:729-44.
41. Dai C, Sampson SB. HSF1: Guardian of Proteostasis in Cancer. Trends Cell Biol 2016;26:17-28.
42. Akerfelt M, Morimoto RI, Sistonen L. Heat shock factors: integrators of cell stress, development and lifespan. Nat Rev Mol Cell Biol 2010;11:545-55.
43. Yoon YJ, Kim JA, Shin KD, Shin DS, Han YM, Lee YJ, et al. KRIBB11 inhibits HSP70 synthesis through inhibition of heat shock factor 1 function by impairing the recruitment of positive transcription elongation factor b to the hsp70 promoter. J Biol Chem 2011;286:1737-47.
44. Pelkonen M, Luostari K, Tengstrom M, Ahonen H, Berdel B, Kataja V, et al. Low expression levels of hepsin and TMPRSS3 are associated with poor breast cancer survival. BMC Cancer 2015;15:431.
45. Tripathi M, Nandana S, Yamashita H, Ganesan R, Kirchhofer D, Quaranta V. Laminin-332 is a substrate for hepsin, a protease associated with prostate cancer progression. J Biol Chem 2008;283:30576-84.
46. Nguyen-Ngoc KV, Cheung KJ, Brenot A, Shamir ER, Gray RS, Hines WC, et al. ECM microenvironment regulates collective migration and local dissemination in normal and malignant mammary epithelium. Proc Natl Acad Sci U S A 2012;109:E2595-604.
47. Jackson EL, Willis N, Mercer K, Bronson RT, Crowley D, Montoya R, et al. Analysis of lung tumor initiation and progression using conditional expression of oncogenic K-ras. Genes Dev 2001;15:3243-8.
48. Brady CA, Jiang D, Mello SS, Johnson TM, Jarvis LA, Kozak MM, et al. Distinct p53 transcriptional programs dictate acute DNA-damage responses and tumor suppression. Cell 2011;145:571-83.
49. Narhi K, Nagaraj AS, Parri E, Turkki R, van Duijn PW, Hemmes A, et al. Spatial aspects of oncogenic signalling determine the response to combination therapy in slice explants from Kras-driven lung tumours. J Pathol 2018;245:101-13.
50. McLaughlin SK, Olsen SN, Dake B, De Raedt T, Lim E, Bronson RT, et al. The RasGAP gene, RASAL2, is a tumor and metastasis suppressor. Cancer Cell 2013;24:365-78.
51. Ganesan R, Zhang Y, Landgraf KE, Lin SJ, Moran P, Kirchhofer D. An allosteric anti-hepsin antibody derived from a constrained phage display library. Protein Eng Des Sel 2012;25:127-33.

52. Ganesan R, Kolumam GA, Lin SJ, Xie MH, Santell L, Wu TD, et al. Proteolytic activation of pro-macrophage-stimulating protein by hepsin. Mol Cancer Res 2011;9:1175-86.
53. Jessani N, Humphrey M, McDonald WH, Niessen S, Masuda K, Gangadharan B, et al. Carcinoma and stromal enzyme activity profiles associated with breast tumor growth in vivo. Proc Natl Acad Sci U S A 2004;101:13756-61.
54. Shields DJ, Niessen S, Murphy EA, Mielgo A, Desgrosellier JS, Lau SK, et al. RBBP9: a tumor-associated serine hydrolase activity required for pancreatic neoplasia. Proc Natl Acad Sci U S A 2010;107:2189-94.
55. Dai C. The heat-shock, or HSF1-mediated proteotoxic stress, response in cancer: from proteomic stability to oncogenesis. Philos Trans R Soc Lond B Biol Sci 2018;373.
56. Lobert VH, Brech A, Pedersen NM, Wesche J, Oppelt A, Malerod L, et al. Ubiquitination of alpha 5 beta 1 integrin controls fibroblast migration through lysosomal degradation of fibronectin-integrin complexes. Dev Cell 2010;19:148-59.
57. Wilkinson DJ, Desilets A, Lin H, Charlton S, Del Carmen Arques M, Falconer A, et al. The serine proteinase hepsin is an activator of pro-matrix metalloproteinases: molecular mechanisms and implications for extracellular matrix turnover. Sci Rep 2017;7:16693.
58. Reid JC, Matsika A, Davies CM, He Y, Broomfield A, Bennett NC, et al. Pericellular regulation of prostate cancer expressed kallikrein-related peptidases and matrix metalloproteinases by cell surface serine proteases. Am J Cancer Res 2017;7:2257-74.

FIGURE LEGENDS

Figure 1. Oncogenic Ras induces hepsin protein and activity. **a** Hepsin was induced in non-malignant MCF10A mammary epithelial cells and the lysates were subjected to immunoblotting with hepsin, HAI-1 and β-tubulin antibodies (left). Whole cell peptide cleavage activity (BOC-QRR-AMC) by ELISA assay while hepsin was induced in non-malignant MCF10A mammary epithelial cells (right). Hepsin was induced for 48 h with 100 ng/ml doxycycline (DOX). hepsin^{IND20}, DOX inducible pINDUCER20-hepsin; -DOX, vehicle control; BOC-QRR-AMC, fluorogenic peptide substrate BOC-Gln-Arg-Arg-AMC (n= 3 biological replicates). **b** Immunoblot analysis of hepsin, HAI-1 and β-tubulin in the lysates prepared from MCF10A cells expressing the defined oncogene or tumor suppressor constructs (MYC, tamoxifen-activated MycER fusion protein; MYCΔ, tamoxifen-treated inactive mutant MycΔER fusion protein as a control; E2F-1, tamoxifen-activated E2F-1ER fusion protein; E2F-1Δ, tamoxifen-treated inactive mutant E2F-1ΔER fusion protein as a control; exp., exposure time. see also Supplementary Fig. 1a, b). **c** Immunoblot analysis of stably KRas^{V12} (left) and KRas^{Wt} (right) overexpressing MCF10A cells with antibodies against hepsin, HAI-1, Ras^{V12} and β-tubulin. **d** Immunoblot analysis of hepsin, HAI-1, Ras^{V12} and β-tubulin in the lysates derived from non-malignant MCF12A mammary epithelial cells (left) and human telomerase immortalized human mammary epithelial cells (HMEC-hT) (right) stably overexpressing HRas^{V12}**. e, f** ELISA assay of cell surface (**e) (**n= 14 to 16 per group of biological replicates) and whole cell (**f**) (n= 3 biological replicates) proteolytic activity in the MCF10A cells stably overexpressing HRas^{V12}. **g** Lysates corresponding to breast cancer cell lines (oncogenic mutations in *RAS*, *PIK3CA* and *RB1* indicated) were subjected to immunoblot analysis of hepsin, HAI-1 and β-tubulin (MCF10As with or w/o HRas^{V12} samples serve as controls). A dot plot graph shows high h-H ratio in RAS/RB1 mutated breast cancer cell lines. **h** Immunoblot analysis of stably KRas^{Wt} overexpressing T47D cells (cell line with intrinsically low hepsin/HAI-1 ratio) for hepsin, HAI-1, pan-Ras and β-tubulin. In **a, b-d, g-h,** h indicates hepsin, H indicates HAI-1 and the h-H ratio indicates hepsin (31 kDa) HAI-1 (66 kDa) loading normalized western blot band intensity ratio in the presented blots. For **a, and e-g** data are presented as mean ± s.e.m. *P*-values were calculated using a two-tailed unpaired Student's t-test. $p^{*}<0.05$, $p^{**}<0.01$.

Figure 2. Oncogenic Ras extends half-life and reduces ubiquitination of hepsin, which is a lysosomal pathway regulated protease. **a** Real-time quantitative RT-PCR analysis of hepsin mRNA expression in MCF10A cells expressing constitutive $HRas^{V12}$ or $KRas^{V12}$ (n= 4 to 5 biological replicates). **b** Cycloheximide (CHX) chase. Immunoblot analysis of hepsin and β-tubulin in the lysates derived from cycloheximide (CHX) treated (50 μg ml^{-1}) MCF10A cells stably overexpressing $HRas^{V12}$. The cells expressing the empty transfer vector were controls. **c** Immunoprecipitation analysis of total ubiquitin. The immunoprecipitation was performed with V5 antibody in cell lysates derived from HEK293FT cells transiently transfected with $KRas^{V12}$, V5 tagged hepsin and control vector (-). **d** Immunoblot analysis of the lysates derived from cells treated with increasing doses of lysosomal inhibitor bafilomycin (24 h): MCF10As (non-malignant control) (from left to right: DMSO, 400 nM, 600 nM), MCF-7s (low hepsin/HAI-1 ratio) (from left to right: DMSO, 100 nM, 200 nM) and T47Ds (low hepsin/HAI-1 ratio) (from left to right: DMSO, 100 nM, 200 nM) with antibodies against hepsin and β-tubulin. Immunoblot panel on the left shows analysis of lysates derived from T47Ds treated with increasing doses of lysosomal inhibitor concanamycin A (from left to right: DMSO, 100 nM, 200 nM; 24 h). **e** Immunofluorescent analysis of hepsin (green) and lysosomal marker lamp2 (red) co-localization in MCF10A cells treated with bafilomycin (500 nM, 24 h), cells stably overexpressing $HRas^{V12}$, and DMSO control (n= 3 to 4 biological replicates, black arrowheads denote co-localization, white in $HRas^{V12}$). Co-localization values are expressed as mean gray value of pixels at minimum of 0.95 intensity ratio (values below the image panels) (ImageJ). **f** Histogram shows hepsin and lamp2 co-localization measured as in (**e**) and normalized to lysosome size (n= 3 to 4 biological replicates, Ctrl = cells expressing the empty vector). In **e,** scale bar represents 20 μm. For **a, e**, **f** data are presented as mean ± s.e.m., *P*-values were calculated using two-tailed unpaired Student's t-test. $p^{*}<0.05$, n.s., not significant.

Figure 3. Ras-MAPK-HSF1 pathway induces hepsin deregulation. **a** Immunoblot analysis of hepsin, HAI-1, Ras^{V12}, phospho-ERK (pERK), total-ERK (ERK) and β-tubulin in cell lysates from MCF10A cells stably overexpressing the doxycycline (DOX)-inducible

pINDUCER20-HRas^{V12} (Ind20-HRas^{V12}, HRas^{V12} A and HRas^{V12} B are different cell culture clones) and CTRL (pINDUCER20 destination plasmid) after DOX induction for indicated time. **b** Normalized (to loading) immunoblot band intensities from (**a**) for HAI-1 at indicated time points (HRas^{V12} compared to CTRL). **c** Illustration of MAPK and PI3K pathway and the inhibitors used here for MEK (AZD6244= MEKi 1.), ERK (SCH772984=ERK1/2i 1.; Erk inh II = ERK1/2i 2.), PI3K(mTOR) (LY294002 and BEZ235), and mTOR (Rapamycin). **d, e** Immunoblot analysis of lysates from MCF10A cells acutely expressing HRas^{V12}, treated with **(d)** MEKi 1., ERK1/2i 1. (both 5 μM, 48 h), or **(e)** ERK1/2 2. (10 μM, 48 h) with antibodies against hepsin, HAI-1, pERK, ERK, Ras^{V12}, GAPDH and β-tubulin (numbers above β-tubulin bands denote loading-normalized hepsin band intensity compared to vehicle). Histogram (below right) shows quantitation of normalized hepsin IB band intensity compared to DMSO treated in **e** of 3 biological replicates. **f, g** Immunoblot analysis of lysates from MCF10A cells acutely expressing HRas^{V12}, treated with **(f)** LY294002 (48 h), **(g)** BEZ235 (500 nM, 48 h) or Rapamycin (20 nM, 48 h) with antibodies against hepsin, phospho-AKT (pAKT), total AKT (AKT), phospho-S6 (pS6), total S6 (S6), and β-tubulin (numbers above β-tubulin bands denote loading-normalized hepsin band intensity compared to vehicle). **h** ELISA analysis (histogram) of BOC-QRR-AMC peptide cleavage activity in MCF10A cells acutely expressing HRas^{V12}, and treated as above with MEKi, ERK1/2i and Rapamycin (mTORi) (20 nM, 48 h) (n= 6-14 biological replicates). **i** Immunoblot analysis of lysates from acute HRas^{V12} (upper blot, Ind20- HRas^{V12}, 100 ng ml^{-1} DOX, 48 h) or stable HRas^{V12} (lower blot) overexpressing MCF10A cells with antibodies for total heat-shock transcription factor 1 (HSF1), Ser326 phosphorylated HSF1 (HSF1 pS326), GAPDH and Ras^{V12}. **j** Immunoblot analysis of HEK 293FT cells transfected with vectors expressing hepsin alone, or hepsin and HSF1 vectors together. **k** Immunoblot analysis of the cell lysates with antibodies against the indicated proteins after heat-shock treatment of HeLa cells (43°C, 1 h). The lysates were harvested after a 5 h of recovery period w/ or w/o HSF1 inhibitor (10 μM KRIBB11). Control sample did not undergo heat-shock treatment. **l, m** Immunoblot analysis of hepsin, HSF1 and β-tubulin in lysates treated with acute lentiviral shRNA (shHSF1 #3) and shCTRL in (**l**) MCF10A-HRas^{V12} cells or **(m)** in Hs578T (Ras mutated, high hepsin/HAI-1 ratio). In **m,** note that the shHSF1 #2 that does not efficiently knock

down HSF1 also leaves hepsin protein level unaffected. **n** Total ubiquitin and hepsin levels (IB). HEK293FT cells were transiently transfected with $KRas^{V12}$, hepsinV5, shHSF1 #3 and shCtrl construct as indicated. V5 tagged hepsin was immunoprecipitated with V5 antibody. In **a,** h indicates hepsin, H indicates HAI-1 and the h-H ratio indicates hepsin (31 kDa) HAI-1 (66 kDa) loading normalized western blot band intensity ratio in the presented blots. For **b**, **e**, and **h,** data are presented as mean ± s.e.m., and *P*-values were calculated using a two-tailed unpaired Student's t-test. $p^{**}<0.01$, $p^{***}<0.001$. n.s., not significant.

Figure 4. Oncogenic Ras abrogates epithelial junctions, which express hepsin. **a** Images of hepsin immunohistochemical staining (brown) in formalin-fixed paraffin embedded (FFPE) human breast cancer specimens. Quantitation of hepsin immunoreactivity in FFPE specimens (upper histogram) and visual assessment of the localization of hepsin immunoreactivity in subtypes of breast cancer (lower histogram) (nuclei were counter-stained with hematoxylin; n= 49 biological replicates, scale bar is 20 μm). **b-d** Representative images of 3 biological replicates of immunofluorescent staining of hepsin and desmoplakin in 2D cultures of breast cancer cell lines (**b**) and non-malignant mammary epithelial cell lines stably overexpressing Ras genes or empty vector controls (**c, d**) and the lowest panel in each figure shows a merged channel image with nuclei (blue). In **b**, co-localization of hepsin and desmoplakin is indicated from with white arrowheads on the magnified inset **(**see Supplementary Fig. 2a). **b** (right) ELISA assay of whole cell BOC-QRR-AMC peptide substrate cleavage activity in Hs578T cells (high hepsin/HAI-1 ratio) and in MCF-7 cells (low hepsin/HAI-1 ratio) (n= 3 biological replicates). **e** Representative images of 3 biological replicates of immunofluorescent staining against hepsin in 3D egg white cultured structures of breast cancer cell lines and MCF10A cell line stably overexpressing mutant Ras or empty vector controls. White arrowheads indicate basal hepsin staining. **f** Analyses of immunofluorescent staining with antibodies against hepsin, laminin-332 β3, laminin-332 γ2 and α6-integrin in 3D egg white cultured structures of MCF10A cell lines stably overexpressing $HRas^{V12}$, MYC ER (+MYC, tamoxifen-activated in the beginning of the 3D culturing) or both $HRas^{V12}$ and MYC ER together ($HRas^{V12}$ +MYC). Controls were empty vector control (control) and MYC ER cells treated with vehicle (-MYC) (n= 3 biological replicates) **(**see Supplementary Fig. 3c, d). White

arrowheads indicate cells bulging out from the 3D structures. **g** Immunoblot analysis of laminin-332 β3 and β-tubulin in lysates derived from control vector expressing MCF10As and MCF10A-HRas^{V12} cells. **h** Immunoblot analysis (left) with antibodies against hepsin and Kras^{G12D} after AdCre-mediated ex vivo activation of Kras^{G12D} in Kras$^{+/LSL-G12D}$ MMECs (total protein level was detected with Ponceau staining) (see also Supplementary Fig. 4b). **i** Immunofluorescent analysis of hepsin in ex vivo AdCre- activated Kras$^{+/LSL-G12D}$ MMEC-derived 3D cultured epithelial structures (n= 3 to 10 mice, 19 to 85 epithelial structures per independent experiment, see also Supplementary Fig. 4c). **j** Immunohistochemical analysis with antibody against hepsin in sporadic lung tumors created by inhalation of AdCre virus in Kras$^{+/LSL-G12D}$; p53$^{-/-}$ double transgenic mice in formalin fixed paraffin embedded (FFPE) sections compared to control lung tissue (n-values denote the number of control lungs and independent tumors) (see also Supplementary Fig. 4e). In **b-f,** scale bars represent 20 μm and the nuclei were visualized with Hoechst (blue). In **e**, **f,** the cells were cultured in 3D for 7 days before immunostaining. For **b**, **f** data are presented as mean ± s.e.m., and for **a** and **c** data are presented as mean ± SD. *P*-values were calculated using a two-tailed unpaired Student's t-test, except in **e** where *P*-value was calculated using a N-1 Two Proportion test. $p^*<0.05$, $p^{**}<0.01$, $p^{***}<0.001$. n.s., not significant.

Figure 5. Ras-MAPK pathway is involved in cellular redistribution of hepsin and disruption of desmosomal and hemidesmosomal junctions **a** Immunofluorescent analysis of hepsin and desmoplakin after acute HRas^{V12} induction in MCF10A cells together with MEK (AZD6244= MEKi 1.) and ERK1/2 (SCH772984=ERK1/2i 1.) inhibitors (both 5 μM, 48 h) (n= 3-6 biological replicates). **b** Immunofluorescent analysis of hepsin, laminin-332 β3, laminin-332 γ2 and α6-integrin in MCF10A 3D epithelial structures acutely expressing HRas^{V12} and treated with MEKi 1. and ERK1/2i 1. (both 5 μM, 3 days) (n= 3-4 biological replicates). **c** Immunohistochemical co-expression analysis of hepsin (brown) and pERK (brown) in serial sections from human breast tumors (68 fields of view in 57 unique patient samples). Nuclei were counterstained with hematoxylin (blue). For monolayer cell culture experiments in **a** HRas^{V12} was induced with 100 ng ml^{-1} of DOX for 48 h at the same time while the drugs were administered to cells, whereas in **(b)** HRas^{V12}

was induced with 900 ng ml^{-1} of DOX at day 4 of 3D culture for 3 days. In **a**, **b,** nuclei were visualized with Hoechst (blue). In **a, b,** scale bar represents 20 μm and in **c** 100 μm. For **a**, **b,** data are presented as mean ± s.e.m., and *P*-values were calculated using a two-tailed unpaired Student's t-test. $p^*<0.05$, $p^{**}<0.01$, $p^{***}<0.001$.

Figure 6. Ras-induced hepsin mediates degradation of desmosomes and basement membrane. **a** shRNA-mediated knockdown of hepsin in $HRas^{V12}$-overexpressing MCF10A cell lysates as detected with antibodies against hepsin, HAI-1, Ras^{V12} and β-tubulin (two different shRNAs for hepsin were used: #1 and #5, shControl= non-target shRNA; h indicates hepsin, H indicates HAI-1 and h-H ratio indicates hepsin (31 kDa)- HAI-1 (66 kDa) loading normalized western blot band intensity ratio; h-H ratioInv means that $HRas^{V12}$-shHepsin #5 band intensities were used as control value in comparison). **b** ELISA assay of whole cell peptide cleavage activity (BOC-QRR-AMC) in $HRas^{V12}$-overexpressing MCF10A cells after shRNA- mediated stable knockdown of hepsin (n= 3 biological replicates). **c** Immunofluorescent analysis with antibodies against hepsin and desmoplakin in MCF10A-$HRas^{V12}$ monolayer cultures stably expressing shHepsin. **d** Immunofluorescent staining for hemidesmosomal and basal lamina components laminin-332 β3, laminin-332 γ2 and α6-integrin after shRNA-mediated stable knockdown of hepsin in 3D cultures of $HRas^{V12}$-overexpressing MCF10A cells (n= 3 to 5 biological replicates). Immunofluorescent staining against hepsin (the leftmost panel) is also shown. **e** Laminin-332 β3 in MCF10A-$HRas^{V12}$ cells after shRNA-mediated knockdown of hepsin. **f** Immunofluorescent analysis of apical polarity through assessment of apical localization of GM130 immunoreactivity in $HRas^{V12}$ overexpressing MCF10As after shRNA- mediated stable knockdown of hepsin (n= 3 to 5 biological replicates). **g** Immunofluorescent analysis of 3D-cultured MCF10A epithelial structures with inducible $HRas^{V12}$ activated by doxycycline (ON, 900 ng ml^{-1}, at day 4) for localization of hemidesmosomal and basal lamina components laminin-332 β3 (green) and α6-integrin (red), and the impact of hepsin function blocking antibody Ab25 (1 μM, at day 4) (n= 4 to 5 biological replicates, see Supplementary Fig. 2). In **c, d, f, g,** nuclei were visualized with Hoechst (blue) and scale bars represent 20 μm. For **b, d, f** and **g,** data are presented as mean ± s.e.m., and *P*-values

were calculated using a two-tailed unpaired Student's t-test. p*<0.05, p**<0.01, p***<0.001.

Figure 7. Hepsin knockdown reduces invasiveness of the MDA-MB-231 tumor xenografts. Analysis of tumor take rate **(a)** and tumor diameter **(b)**. MDA-MB-231 cells were lentivirally engineered to express denoted shRNA constructs and transplanted subcutaneously; $n^{shControl}$ = 6 sites per 4 mice, $n^{shHepsin\ \#1}$= 5 sites per 5 mice, $n^{shHepsin\ \#5}$= 5 sites per 5 mice. **c** Percent of tumor area invaded into muscle or fat tissue (red dotted line = invasion into muscle/fat; black line = edge of the main tumor mass; M, muscle; F, fat; T, tumor; T/M, tumor invaded into muscle; T/F, tumor invaded into fat; $n^{shControl}$ = 4, $n^{shHepsin}$ = 3). **d** Immunohistochemical staining with collagen IV and histoscore in MDA-MB-231 xenograft tumors lentivirally engineered to express shRNA constructs ($n^{shControl}$ = 39 fields of view in 4 tumors and $n^{shHepsin}$ = 24 fields of view in 3 tumors). Scale bars represent 500 μm for **c** and 50 μm for **d**. For **b-d,** data are presented as mean ± s.e.m., and *P*-values were calculated using a two-tailed unpaired Student's t-test. p*<0.05, p***<0.05, n.s., not significant. **e** Schematic model of hepsin deregulation by oncogenic Ras. The MAPK pathway drives the Ras-mediated effects on hepsin through the master regulator of proteostasis, HSF1, which causes the stabilization of active form of the hepsin protein. Consequently, hepsin is upregulated and redistributed in the cells, leading to deterioration of desmosomes and hemidesmosomes.

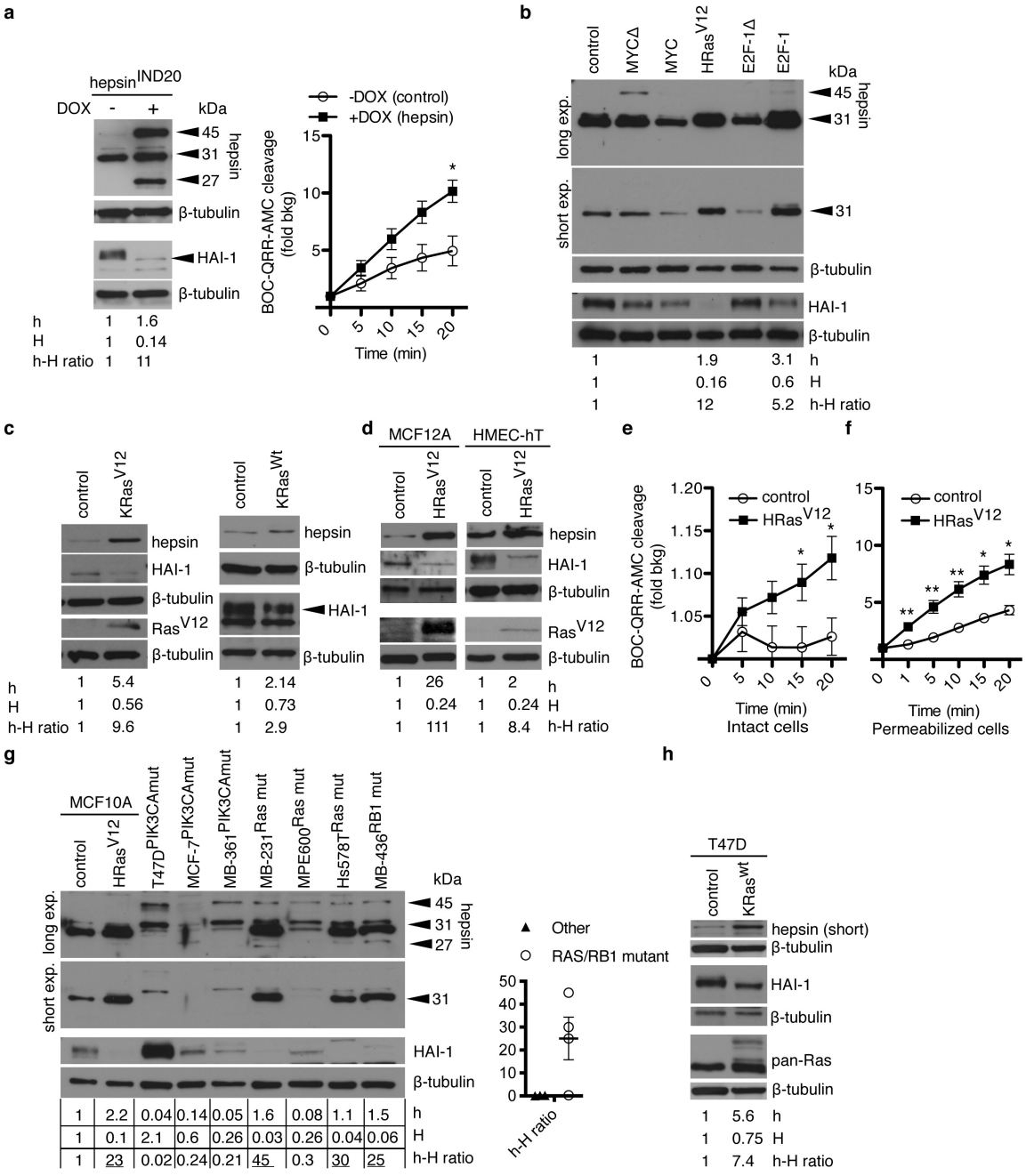
a
hepsin IND20
DOX - +
kDa
45
31
27
hepsin
β-tubulin
HAI-1
β-tubulin
h 1 1.6
H 1 0.14
h-H ratio 1 11
-DOX (control)
+DOX (hepsin)
BOC-QRR-AMC cleavage (fold bkg)
Time (min)
b
control
MYCΔ
MYC
HRasV12
E2F-1Δ
E2F-1
kDa
long exp.
short exp.
hepsin
45
31
β-tubulin
HAI-1
1 1.9 3.1 h
1 0.16 0.6 H
1 12 5.2 h-H ratio
c
control
KRasV12
control
KRasWt
hepsin
HAI-1
β-tubulin
RasV12
h 1 5.4 1 2.14
H 1 0.56 1 0.73
h-H ratio 1 9.6 1 2.9
d
MCF12A
HMEC-hT
control
HRasV12
control
HRasV12
hepsin
HAI-1
β-tubulin
RasV12
h 1 26 1 2
H 1 0.24 1 0.24
h-H ratio 1 111 1 8.4
e
BOC-QRR-AMC cleavage (fold bkg)
control
HRasV12
Time (min)
Intact cells
f
control
HRasV12
Time (min)
Permeabilized cells
g
MCF10A
control
HRasV12
T47D PIK3CAmut
MCF-7 PIK3CAmut
MB-361 PIK3CAmut
MB-231 Ras mut
MPE600 Ras mut
Hs578T Ras mut
MB-436 RB1 mut
kDa
long exp.
short exp.
hepsin
45
31
27
HAI-1
β-tubulin
h 1 2.2 0.04 0.14 0.05 1.6 0.08 1.1 1.5
H 1 0.1 2.1 0.6 0.26 0.03 0.26 0.04 0.06
h-H ratio 1 23 0.02 0.24 0.21 45 0.3 30 25
Other
RAS/RB1 mutant
h-H ratio
h
T47D
control
KRaswt
hepsin (short)
β-tubulin
HAI-1
β-tubulin
pan-Ras
β-tubulin
1 5.6 h
1 0.75 H
1 7.4 h-H ratio

FIGURE 1.

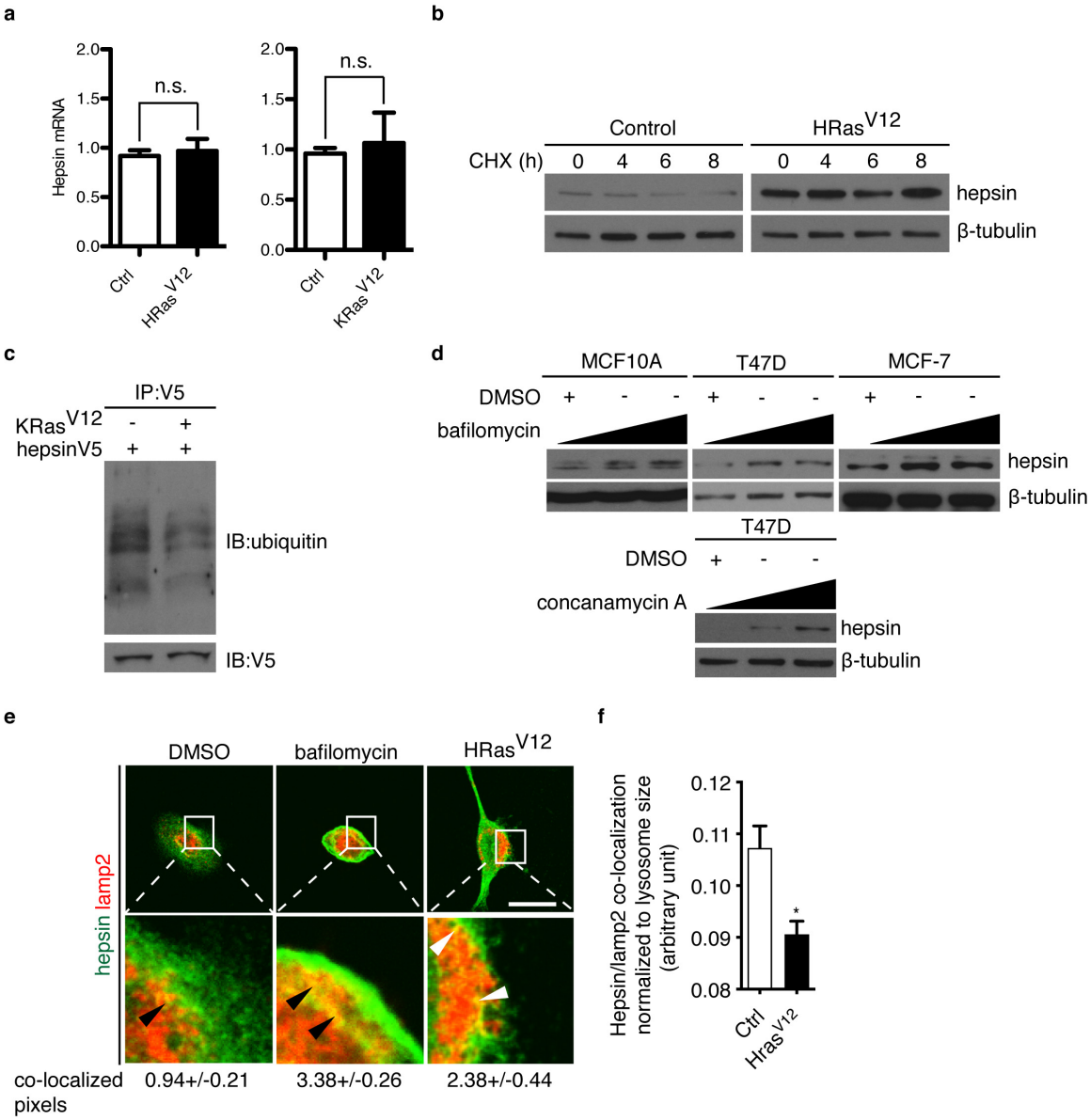
a
Hepsin mRNA
2.0
1.5
1.0
0.5
0.0
n.s.
Ctrl
HRas V12
KRas V12
b
Control
HRasV12
CHX (h)
0 4 6 8
hepsin
β-tubulin
c
IP:V5
KRasV12
hepsinV5
IB:ubiquitin
IB:V5
d
MCF10A
T47D
MCF-7
DMSO
bafilomycin
concanamycin A
e
DMSO
bafilomycin
HRasV12
hepsin lamp2
co-localized pixels
0.94+/-0.21
3.38+/-0.26
2.38+/-0.44
f
Hepsin/lamp2 co-localization normalized to lysosome size (arbitrary unit)
0.12
0.11
0.10
0.09
0.08

FIGURE 2.

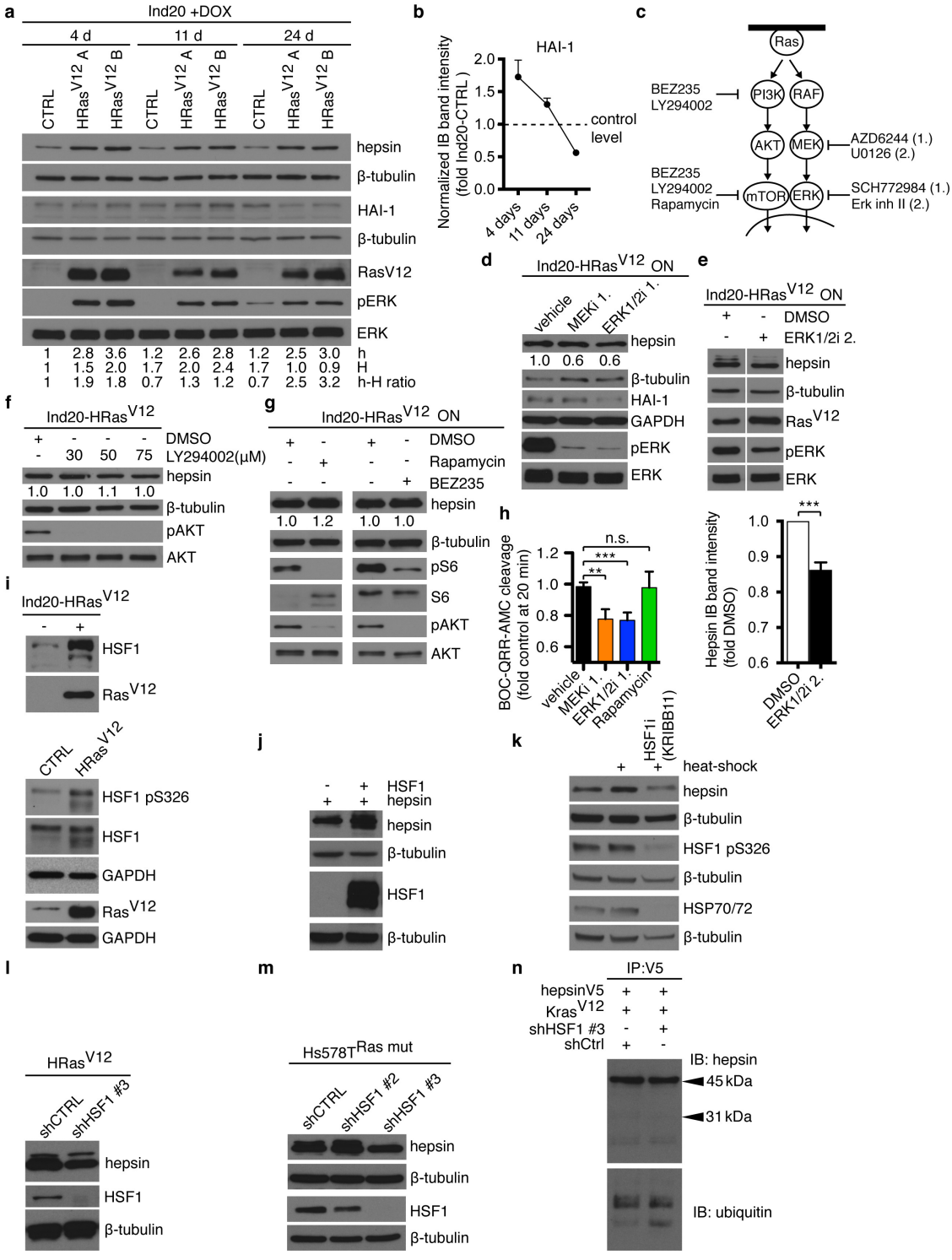
a
Ind20 +DOX
4 d
11 d
24 d
CTRL
HRasV12 A
HRasV12 B
hepsin
β-tubulin
HAI-1
RasV12
pERK
ERK
h
H
h-H ratio
b
HAI-1
Normalized IB band intensity (fold Ind20-CTRL)
control level
4 days
11 days
24 days
c
Ras
PI3K
RAF
AKT
MEK
mTOR
ERK
BEZ235
LY294002
Rapamycin
AZD6244 (1.)
U0126 (2.)
SCH772984 (1.)
Erk inh II (2.)
d
Ind20-HRasV12 ON
vehicle
MEKi 1.
ERK1/2i 1.
GAPDH
e
DMSO
ERK1/2i 2.
f
Ind20-HRasV12
LY294002(μM)
pAKT
AKT
g
Rapamycin
BEZ235
pS6
S6
h
BOC-QRR-AMC cleavage (fold control at 20 min)
n.s.
Hepsin IB band intensity (fold DMSO)
i
HSF1
HSF1 pS326
j
k
HSF1i (KRIBB11)
heat-shock
HSP70/72
l
HRasV12
shCTRL
shHSF1 #3
m
Hs578TRas mut
shHSF1 #2
n
IP:V5
hepsinV5
KrasV12
shHSF1 #3
shCtrl
IB: hepsin
45 kDa
31 kDa
IB: ubiquitin

FIGURE 3.

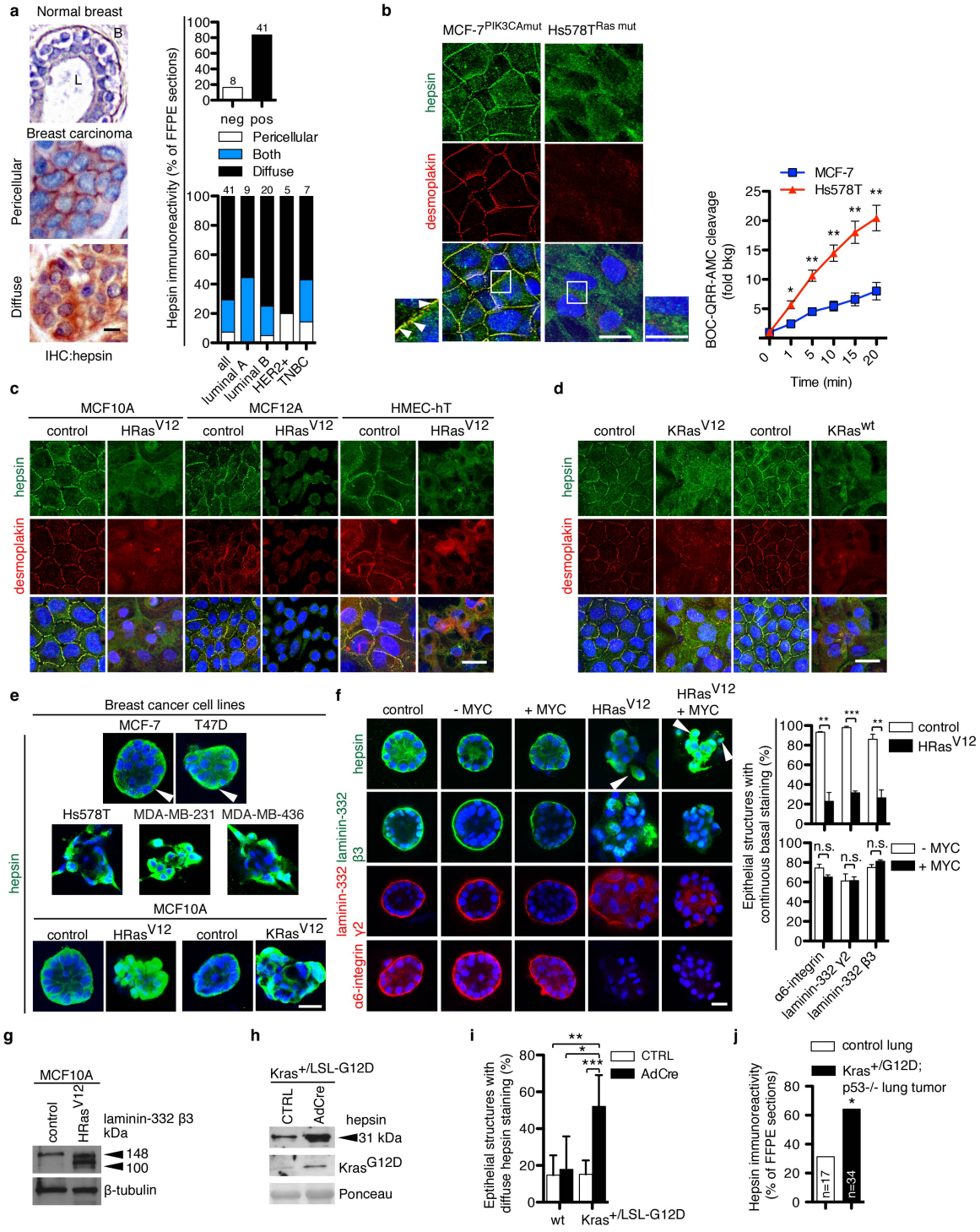
a
Normal breast
B
L
Breast carcinoma
Pericellular
Diffuse
IHC:hepsin
Hepsin immunoreactivity (% of FFPE sections)
41
8
neg pos
Pericellular
Both
Diffuse
41 9 20 5 7
all
luminal A
luminal B
HER2+
TNBC
b
MCF-7PIK3CAmut
Hs578TRas mut
hepsin
desmoplakin
BOC-QRR-AMC cleavage (fold bkg)
MCF-7
Hs578T
Time (min)
c
MCF10A
MCF12A
HMEC-hT
control
HRasV12
hepsin
desmoplakin
d
control
KRasV12
control
KRaswt
hepsin
desmoplakin
e
Breast cancer cell lines
MCF-7
T47D
Hs578T
MDA-MB-231
MDA-MB-436
hepsin
MCF10A
control
HRasV12
control
KRasV12
f
control
- MYC
+ MYC
HRasV12
HRasV12 + MYC
hepsin
laminin-332 β3
laminin-332 γ2
α6-integrin
Epithelial structures with continuous basal staining (%)
control
HRasV12
- MYC
+ MYC
n.s.
α6-integrin
laminin-332 γ2
laminin-332 β3
g
MCF10A
control
HRasV12
laminin-332 β3 kDa
148
100
β-tubulin
h
Kras+/LSL-G12D
CTRL
AdCre
hepsin
31 kDa
KrasG12D
Ponceau
i
Epithelial structures with diffuse hepsin staining (%)
CTRL
AdCre
wt
Kras+/LSL-G12D
j
control lung
Kras+/G12D; p53-/- lung tumor
Hepsin immunoreactivity (% of FFPE sections)
n=17
n=34

FIGURE 4.

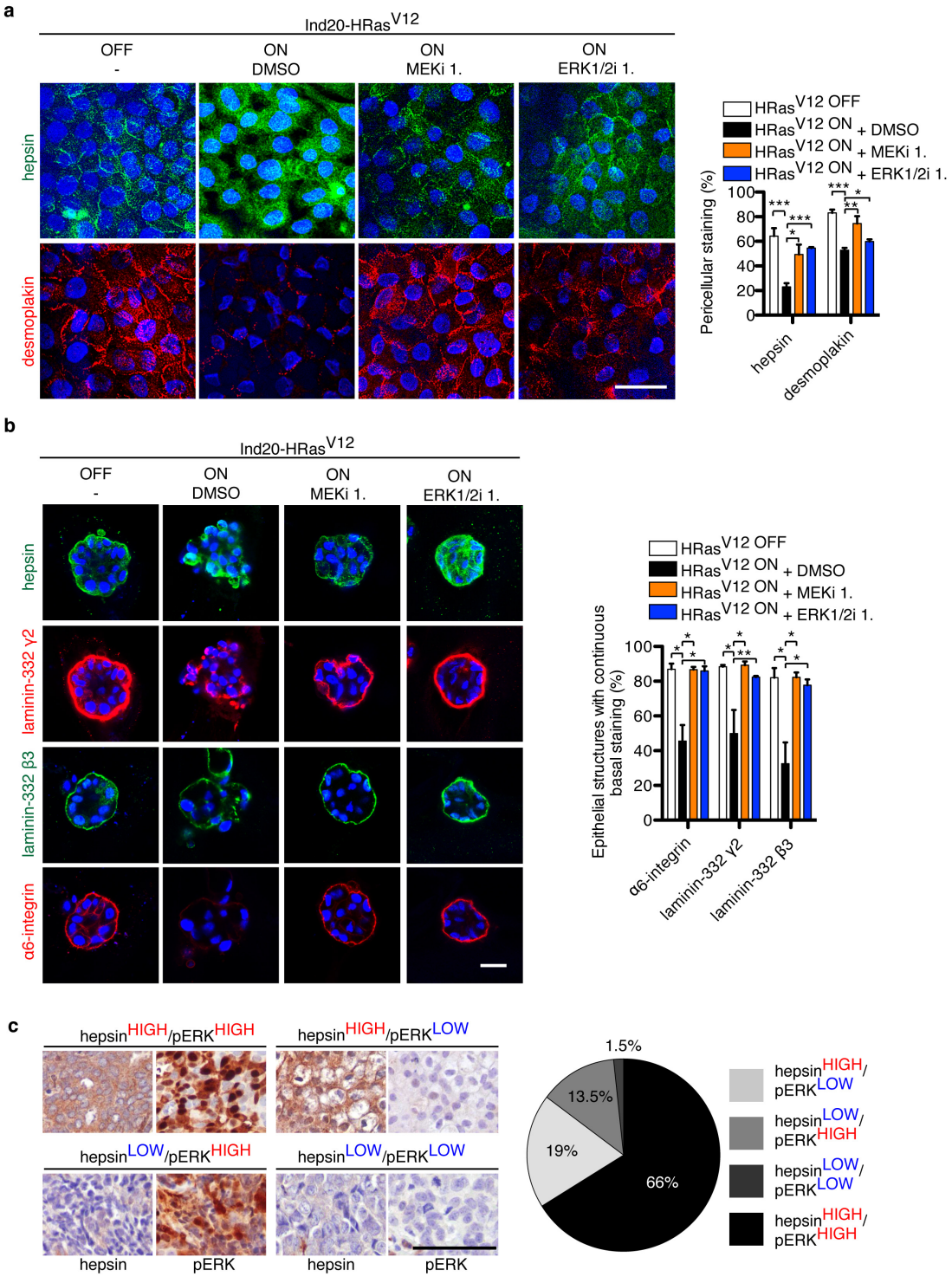
a
Ind20-HRasV12
OFF
-
ON
DMSO
ON
MEKi 1.
ON
ERK1/2i 1.
hepsin
desmoplakin
HRasV12 OFF
HRasV12 ON + DMSO
HRasV12 ON + MEKi 1.
HRasV12 ON + ERK1/2i 1.
Pericellular staining (%)
100
80
60
40
20
0
***
*
hepsin
desmoplakin
b
Ind20-HRasV12
OFF
-
ON
DMSO
ON
MEKi 1.
ON
ERK1/2i 1.
hepsin
laminin-332 γ2
laminin-332 β3
α6-integrin
HRasV12 OFF
HRasV12 ON + DMSO
HRasV12 ON + MEKi 1.
HRasV12 ON + ERK1/2i 1.
Epithelial structures with continuous basal staining (%)
100
80
60
40
20
0
α6-integrin
laminin-332 γ2
laminin-332 β3
c
hepsinHIGH/pERKHIGH
hepsinHIGH/pERKLOW
hepsinLOW/pERKHIGH
hepsinLOW/pERKLOW
hepsin
pERK
1.5%
13.5%
19%
66%
hepsinHIGH/ pERKLOW
hepsinLOW/ pERKHIGH
hepsinLOW/ pERKLOW
hepsinHIGH/ pERKHIGH

FIGURE 5.

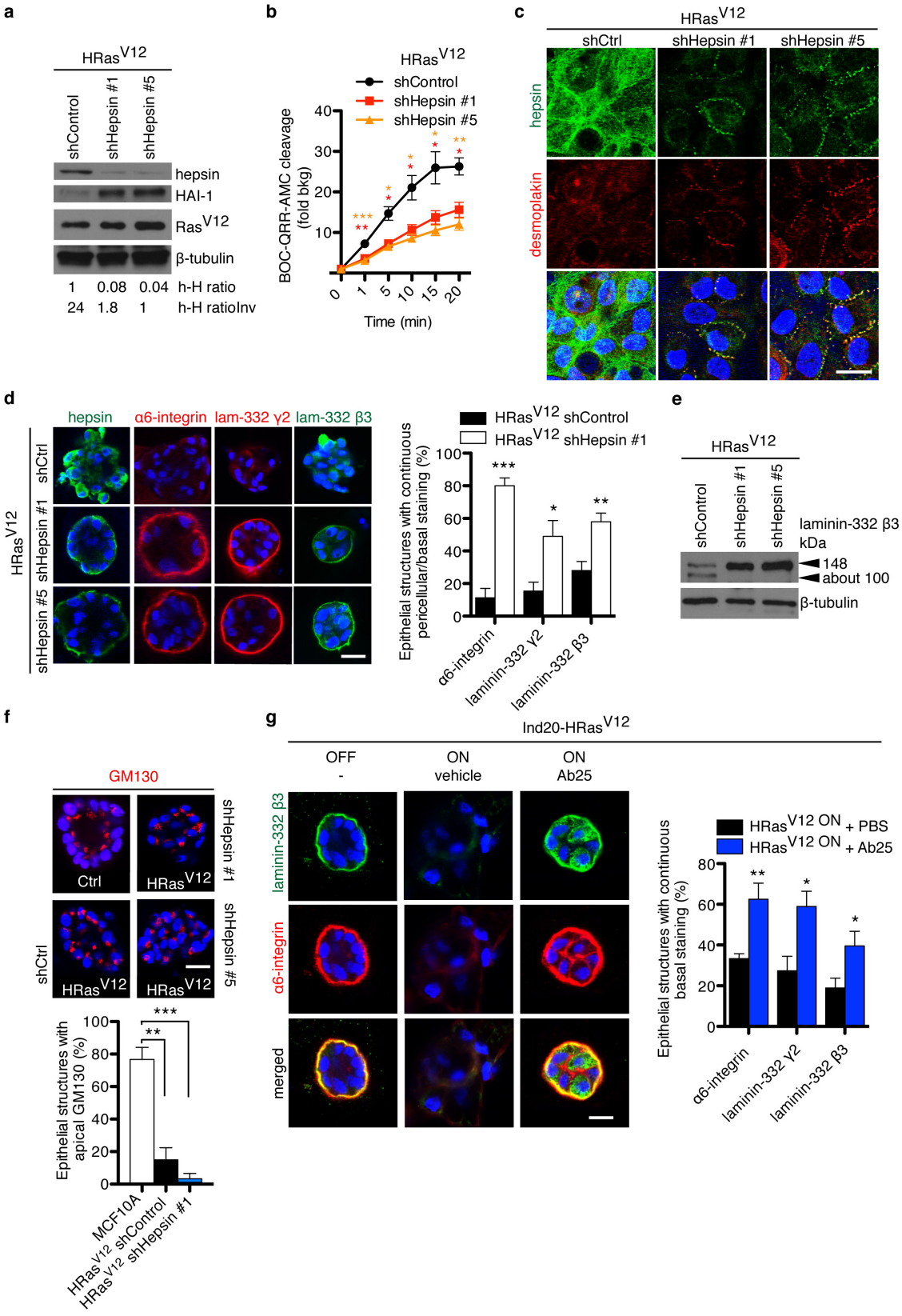
a
HRasV12
shControl
shHepsin #1
shHepsin #5
hepsin
HAI-1
RasV12
β-tubulin
1 0.08 0.04 h-H ratio
24 1.8 1 h-H ratioInv
b
HRasV12
shControl
shHepsin #1
shHepsin #5
BOC-QRR-AMC cleavage (fold bkg)
Time (min)
c
HRasV12
shCtrl
shHepsin #1
shHepsin #5
hepsin
desmoplakin
d
hepsin
α6-integrin
lam-332 γ2
lam-332 β3
HRasV12
shCtrl
shHepsin #1
shHepsin #5
HRasV12 shControl
HRasV12 shHepsin #1
Epithelial structures with continuous pericellular/basal staining (%)
α6-integrin
laminin-332 γ2
laminin-332 β3
e
HRasV12
shControl
shHepsin #1
shHepsin #5
laminin-332 β3
kDa
148
about 100
β-tubulin
f
GM130
Ctrl
HRasV12
shCtrl
shHepsin #1
shHepsin #5
Epithelial structures with apical GM130 (%)
MCF10A
HRasV12 shControl
HRasV12 shHepsin #1
g
Ind20-HRasV12
OFF
-
ON
vehicle
ON
Ab25
laminin-332 β3
α6-integrin
merged
HRasV12 ON + PBS
HRasV12 ON + Ab25
Epithelial structures with continuous basal staining (%)
α6-integrin
laminin-332 γ2
laminin-332 β3

FIGURE 6.

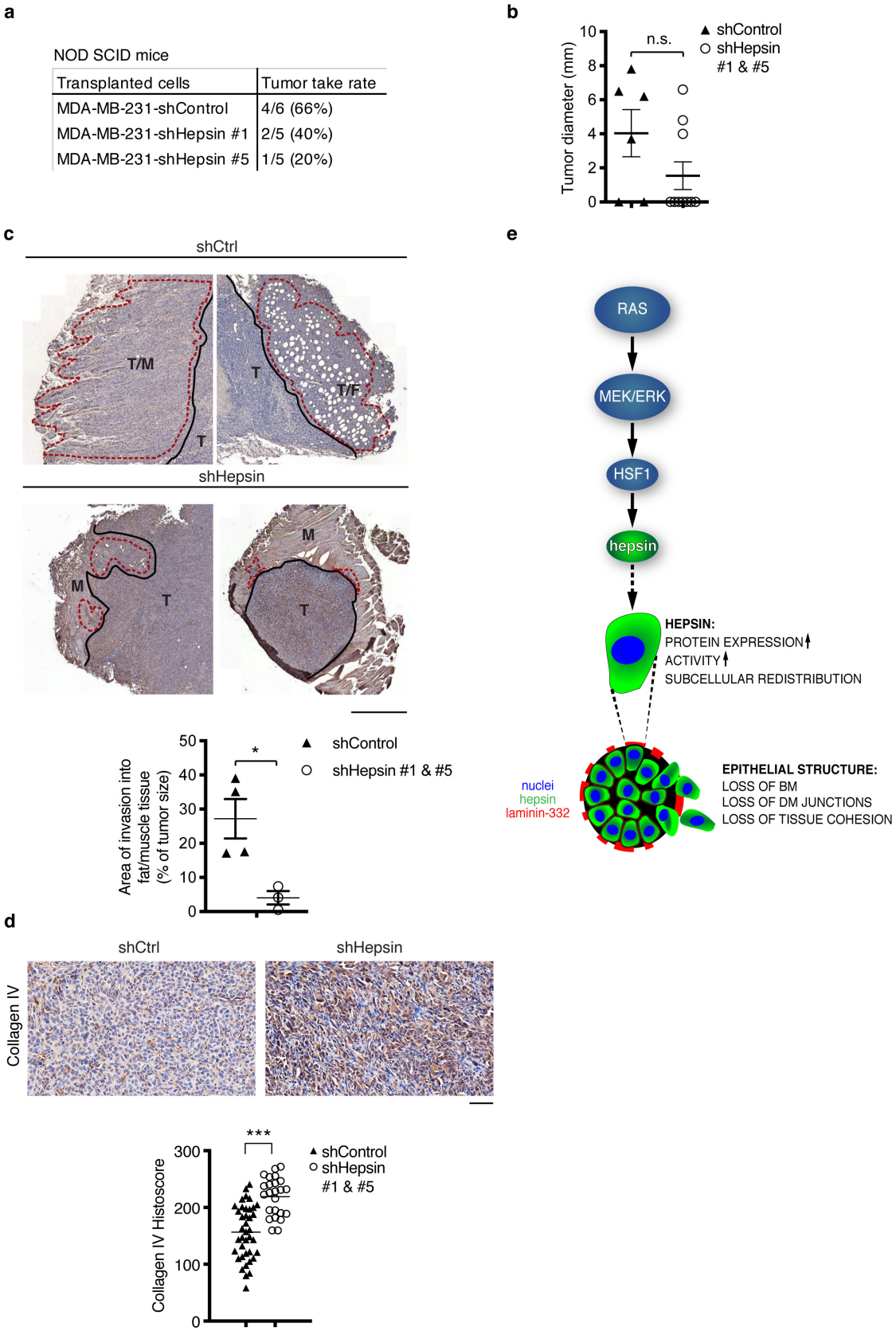
a
NOD SCID mice
Transplanted cells | Tumor take rate
MDA-MB-231-shControl | 4/6 (66%)
MDA-MB-231-shHepsin #1 | 2/5 (40%)
MDA-MB-231-shHepsin #5 | 1/5 (20%)
b
Tumor diameter (mm)
n.s.
shControl
shHepsin #1 & #5
c
shCtrl
T/M
T
T/F
shHepsin
M
T
Area of invasion into fat/muscle tissue (% of tumor size)
*
shControl
shHepsin #1 & #5
d
shCtrl
shHepsin
Collagen IV
***
Collagen IV Histoscore
shControl
shHepsin #1 & #5
e
RAS
MEK/ERK
HSF1
hepsin
HEPSIN:
PROTEIN EXPRESSION
ACTIVITY
SUBCELLULAR REDISTRIBUTION
nuclei
hepsin
laminin-332
EPITHELIAL STRUCTURE:
LOSS OF BM
LOSS OF DM JUNCTIONS
LOSS OF TISSUE COHESION

FIGURE 7.